Supplemental Material can be found at:
http://www.jbc.org/content/suppl/2008/12/23/M806853200.DC1.html

20. Moriki, N., Ito, M., Seko, T., Kureishi, Y., Okamoto, R., Nakakuki, T., Kongo, M., Isaka, N., Kaibuchi, K., and Nakano, T. (2004) *Hypertens. Res.* **27,** 263–270
21. Kandabashi, T., Shimokawa, H., Miyata, K., Kunihiro, I., Kawano, Y., Fukata, Y., Higo, T., Egashira, K., Takahashi, S., Kaibuchi, K., and Takeshita, A. (2000) *Circulation* **101,** 1319–1323
22. Sato, M., Tani, E., Fujikawa, H., and Kaibuchi, K. (2000) *Circ. Res.* **87,** 195–200
23. Guilluy, C., Sauzeau, V., Rolli-Derkinderen, M., Guerin, P., Sagan, C., Pacaud, P., and Loirand, G. (2005) *Br. J. Pharmacol.* **146,** 1010–1018
24. Kimura, K., Fukata, Y., Matsuoka, Y., Bennett, V., Matsuura, Y., Okawa, K., Iwamatsu, A., and Kaibuchi, K. (1998) *J. Biol. Chem.* **273,** 5542–5548
25. Amano, M., Ito, M., Kimura, K., Fukata, Y., Chihara, K., Nakano, T., Matsuura, Y., and Kaibuchi, K. (1996) *J. Biol. Chem.* **271,** 20246–20249
26. Ligeti, E., and Settleman, J. (2006) *Methods Enzymol.* **406,** 104–117
27. Ren, X. D., Kiosses, W. B., and Schwartz, M. A. (1999) *EMBO J.* **18,** 578–585
28. Ridley, A. J., Self, A. J., Kasmi, F., Paterson, H. F., Hall, A., Marshall, C. J., and Ellis, C. (1993) *EMBO J.* **12,** 5151–5160
29. Settleman, J., Narasimhan, V., Foster, L. C., and Weinberg, R. A. (1992) *Cell* **69,** 539–549
30. Vincent, S., and Settleman, J. (1999) *Eur. J. Cell Biol.* **78,** 539–548
31. Mammoto, A., Huang, S., and Ingber, D. E. (2007) *J. Cell Sci.* **120,** 456–467
32. Chardin, P. (2006) *Nat. Rev. Mol. Cell. Biol.* **7,** 54–62
33. Nobes, C. D., Lauritzen, I., Mattei, M. G., Paris, S., Hall, A., and Chardin, P. (1998) *J. Biol. Chem.* **141,** 187–197
34. Harada, A., Katoh, H., and Negishi, M. (2005) *J. Biol. Chem.* **280,** 18418–18424
35. Wennerberg, K., Forget, M. A., Ellerbroek, S. M., Arthur, W. T., Burridge, K., Settleman, J., Der, C. J., and Hansen, S. H. (2003) *Curr. Biol.* **13,** 1106–1115
36. Hynynen, M. M., and Khalil, R. A. (2006) *Recent Patents Cardiovasc. Drug Discov.* **1,** 95–108
37. Worth, N. F., Campbell, G. R., Campbell, J. H., and Rolfe, B. E. (2004) *Cell Motil. Cytoskeleton* **59,** 189–200
38. Gohla, A., Schultz, G., and Offermanns, S. (2000) *Circ. Res.* **87,** 221–227
39. Hersch, E., Huang, J., Grider, J. R., and Murthy, K. S. (2004) *Am. J. Physiol.* **287,** C1209–C1218
40. Agapitov, A. V., and Haynes, W. G. (2002) *J. Renin Angiotensin Aldosterone Syst.* **3,** 1–15

Downloaded from www.jbc.org at CHUOU TOSHOKAN, on April 25, 2010

Published July 13, 2009

ARTICLE

Mobile DHHC palmitoylating enzyme mediates activity-sensitive synaptic targeting of PSD-95

Jun Noritake,[1] Yuko Fukata,[1,2] Tsuyoshi Iwanaga,[1] Naoki Hosomi,[3] Ryouhei Tsutsumi,[1] Naoto Matsuda,[1] Hideki Tani,[4] Hiroko Iwanari,[3] Yasuhiro Mochizuki,[3] Tatsuhiko Kodama,[3] Yoshiharu Matsuura,[4] David S. Bredt,[5] Takao Hamakubo,[3] and Masaki Fukata[1,2]

[1]Division of Membrane Physiology, Department of Cell Physiology, National Institute for Physiological Sciences, Okazaki, Aichi 444-8787, Japan
[2]Precursory Research for Embryonic Science and Technology, Japan Science and Technology Agency, Chiyoda-ku, Tokyo 102-0075, Japan
[3]Laboratory for Systems Biology and Medicine, Research Center for Advanced Science and Technology, The University of Tokyo, Meguro-ku, Tokyo 153-8904, Japan
[4]Department of Molecular Virology, Research Institute for Microbial Diseases, Osaka University, Suita, Osaka 565-0871, Japan
[5]Department of Neuroscience, Eli Lilly and Company, Indianapolis, IN 46285

Protein palmitoylation is the most common posttranslational lipid modification; its reversibility mediates protein shuttling between intracellular compartments. A large family of DHHC (Asp-His-His-Cys) proteins has emerged as protein palmitoyl acyltransferases (PATs). However, mechanisms that regulate these PATs in a physiological context remain unknown. In this study, we efficiently monitored the dynamic palmitate cycling on synaptic scaffold PSD-95. We found that blocking synaptic activity rapidly induces PSD-95 palmitoylation and mediates synaptic clustering of PSD-95 and associated AMPA (α-amino-3-hydroxy-5-methyl-4-isoxazole propionic acid)-type glutamate receptors. A dendritically localized DHHC2 but not the Golgi-resident DHHC3 mediates this activity-sensitive palmitoylation. Upon activity blockade, DHHC2 translocates to the postsynaptic density to transduce this effect. These data demonstrate that individual DHHC members are differentially regulated and that dynamic recruitment of protein palmitoylation machinery enables compartmentalized regulation of protein trafficking in response to extracellular signals.

Introduction

Posttranslational modification, including phosphorylation, ubiquitination, and lipid modification, adds functional regulation to proteins beyond genomic information. Lipid modification increases protein hydrophobicity and plays a critical role in protein trafficking, targeting, and function. Thioester-linked palmitate modifies signaling proteins, enzymes, cytoskeletal proteins, ion channels, and scaffolding proteins and is involved in diverse aspects of cellular signaling (El-Husseini and Bredt, 2002; Resh, 2006; Linder and Deschenes, 2007). Recent global proteomic analyses have further expanded the known complement of palmitoylated proteins (Roth et al., 2006; Kang et al., 2008). Palmitoylation is unique in that it is a reversible modification and is proposed to be regulated by specific extracellular signals. Recent cell biological analyses revealed that some palmitoyl substrates such as small GTPases, Harvey Ras/neuroblastoma Ras (Rocks et al., 2005), and trimeric G proteins Gαo (Chisari et al., 2007)/Gαq (Tsutsumi et al., 2009) constitutively shuttle between the plasma membrane and the Golgi membrane by a palmitoylation/depalmitoylation cycle. This palmitate cycling generates and maintains the specific intracellular compartmentalization of substrates in nonpolarized cells (Rocks et al., 2006).

The postsynaptic scaffolding protein PSD-95 represents a major palmitoylated protein in neurons and plays critical roles in synaptogenesis and synaptic plasticity (Migaud et al., 1998; El-Husseini et al., 2000; Kennedy, 2000; Kim and Sheng, 2004; Funke et al., 2005). PSD-95 provides a platform for the postsynaptic clustering of crucial synaptic proteins, including AMPA (α-amino-3-hydroxy-5-methyl-4-isoxazole propionic

Correspondence to Masaki Fukata: mfukata@nips.ac.jp

Abbreviations used in this paper: 2-BP, 2-bromopalmitate; ABE, acyl-biotin exchange; AMPAR, AMPA receptor; βME, β-mercaptoethanol; CCD, charge-coupled device; CHX, cycloheximide; CM, chloroform-methanol; DIV, day in vitro; DN, dominant-negative; Kyn, kynurenic acid; LB, lysis buffer; miRNA, microRNA; NEM, *N*-ethyl-maleimide; NMDA, *N*-methyl-D-aspartate; PAT, palmitoyl acyltransferase; PPT, palmitoyl protein thioesterase; TARP, transmembrane AMPAR regulatory protein; TIRFM, total internal reflection fluorescence microscopy; TTX, tetrodotoxin; WT, wild type.

© 2009 Noritake et al. This article is distributed under the terms of an Attribution–Noncommercial–Share Alike–No Mirror Sites license for the first six months after the publication date (see http://www.jcb.org/misc/terms.shtml). After six months it is available under a Creative Commons License (Attribution–Noncommercial–Share Alike 3.0 Unported license, as described at http://creativecommons.org/licenses/by-nc-sa/3.0/).

Supplemental Material can be found at:
http://jcb.rupress.org/content/suppl/2009/07/13/jcb.200903101.DC1.html

The Rockefeller University Press $30.00
J. Cell Biol. Vol. 186 No. 1 147–160
www.jcb.org/cgi/doi/10.1083/jcb.200903101

THE JOURNAL OF CELL BIOLOGY

Downloaded from jcb.rupress.org on April 25, 2010

Published July 13, 2009

acid) and *N*-methyl-D-aspartate (NMDA)-type glutamate receptors and cell adhesion molecules. The postsynaptic targeting of PSD-95 depends on protein palmitoylation (Topinka and Bredt, 1998). Importantly, palmitate cycling on PSD-95 is dynamically regulated by receptor activation (El-Husseini et al., 2002). Upon glutamate receptor stimulation, accelerated depalmitoylation of PSD-95 dissociates PSD-95 from postsynaptic sites and causes AMPA receptor (AMPAR) endocytosis. This receptor activation–induced depalmitoylation has also been reported in Gα (Wedegaertner and Bourne, 1994). Thus, agonist-dependent depalmitoylation down-regulates synaptic strength and G protein signaling. However, it is not yet clear whether addition of palmitate to proteins is accelerated in response to extracellular signals.

The dynamic regulation of palmitate cycling should be finely tuned by palmitoyl acyltransferases (PATs) and palmitoyl protein thioesterases (PPTs). Transmembrane proteins containing a DHHC (Asp-His-His-Cys) Cys–rich domain (DHHC proteins) have recently emerged as PATs in yeast (Bartels et al., 1999; Lobo et al., 2002; Roth et al., 2002; Linder and Deschenes, 2004). At least 23 mammalian DHHC proteins exist, and a systematic screening method has identified specific enzyme–substrate pairs (Fukata et al., 2004; Fang et al., 2006; Fernandez-Hernando et al., 2006; Fukata et al., 2006; Ponimaskin et al., 2008; Tsutsumi et al., 2009). The DHHC family is present in species ranging from yeast to human and to plants (Hemsley et al., 2005; Hemsley and Grierson, 2008). Several DHHC genes are associated with diseases, including cancers (Oyama et al., 2000), schizophrenia (Mukai et al., 2004, 2008), mental retardation (Mansouri et al., 2005; Raymond et al., 2007), and Huntington's (Yanai et al., 2006). Although the large DHHC family plays essential roles in a range of physiological functions, how the DHHC PAT family is regulated and thereby dynamically controls palmitate cycling remains uncertain.

In this study, we found that suppression of neuronal activity induces palmitoylation and synaptic accumulation of PSD-95. This activity-sensitive PSD-95 palmitoylation recruits synaptic AMPARs. Dendritically localized DHHC2 mediates this rapid synaptic palmitoylation of PSD-95. In contrast, Golgi-resident DHHC3 constitutively palmitoylates PSD-95. These experiments indicate that large DHHC family members are individually regulated, which enables their participation in specific physiological processes such as synaptic plasticity.

Results

Total internal reflection fluorescence microscopy (TIRFM) reveals the synaptic accumulation of PSD-95 upon activity blockade

To follow changes in synaptic PSD-95 accumulation over time, we first performed time-lapse imaging of cultured hippocampal neurons transfected with PSD-95–GFP by TIRFM, which excites only molecules within 100 nm of the cover glass. TIRFM preferentially visualizes wild-type (WT) PSD-95–GFP as discrete punctae on dendrites, which are not seen with cytosolic palmitoylation–deficient (CS) mutant PSD-95 or GFP (Fig. 1, A and B). We confirmed comparable expression levels of PSD-95 (WT) and PSD-95 (CS) in transfected culture (Fig. 1 B). These data confirm that palmitoylation mediates membrane trafficking and synaptic clustering of PSD-95 (Topinka and Bredt, 1998). Because PSD-95 visualized by TIRFM apposes presynaptic synaptophysin and VGLUT1 and overlaps postsynaptic NR1 NMDA receptor (Fig. 1 C), TIRFM tracks synaptic PSD-95. When ionotropic glutamate receptor activity was blocked by kynurenic acid (Kyn), the intensity of PSD-95–GFP by TIRFM steadily increased over 2 h, whereas the intensity of PSD-95 (CS) did not change (Fig. 1, D and E; and Video 1). This Kyn-induced PSD-95 increase was blocked by coapplication of 2-bromopalmitate (2-BP), which is a palmitoyl acyl transfer inhibitor. PSD-95 signals did not detectably change within 2 h of 2-BP treatment alone (Fig. 1 E). These results indicate that newly occurring palmitoylation mediates this synaptic accumulation of PSD-95. Tetrodotoxin (TTX), a blocker of action potentials, also increased PSD-95 accumulation. The dynamic change of PSD-95 intensity was specific to palmitoylation as the localizations of GFP-Rac1-CLLL (Cys-Leu-Leu-Leu), a geranylgeranylated CaaL motif, and synaptophysin-GFP, a presynaptic protein, did not change upon Kyn treatment (Fig. 1 E). Synaptic PSD-95 accumulation upon activity blockade was also confirmed by antibody staining of native PSD-95 (see Fig. 4, C and D). The effect of Kyn or TTX on PSD-95 accumulation does not reflect newly synthesized PSD-95, as cycloheximide (CHX), an inhibitor of protein synthesis, did not affect the Kyn- or TTX-induced PSD-95 increase (Fig. S1, A and B; and Video 2). Thus, PSD-95 palmitoylation increases at the postsynaptic membrane upon activity blockade. These results are complementary to receptor activation–induced depalmitoylation of PSD-95 (El-Husseini et al., 2002).

The DHHC2/15 subfamily of PSD-95 palmitoylating enzymes is regulated by synaptic activity

To monitor PSD-95 palmitoylation biochemically, we used the acyl-biotin exchange (ABE) method (Roth et al., 2006; Kang et al., 2008). We confirmed that this method specifically identified palmitoylated proteins, including PSD-95, in heterologous cells (Fig. S2 A). As previously reported (El-Husseini et al., 2002), treating neurons for 12 h with 2-BP reduced PSD-95 palmitoylation (palmitoylated PSD-95 = 13 ± 15% of control cells; $P < 0.001$; Fig. 2 A). When we treated neurons for 2 h with Kyn, the amount of palmitoylated PSD-95 significantly increased (198 ± 13% of control cells; $P < 0.001$; Fig. 2, A and B). Blocking glutamate receptors with a combination of APV (D-[-]-2-amino-5-phosphonopentanoic acid), which blocks NMDA receptors, and CNQX (6-cyano-7-nitroquinoxaline-2,3-dione), which blocks AMPARs, also enhanced PSD-95 palmitoylation within 2 h (palmitoylated PSD-95 = 184 ± 23% of control cells; $P < 0.01$). 2-BP blocked the rapid enhancement of PSD-95 palmitoylation, indicating that inhibition of depalmitoylation is not solely responsible and that newly occurring palmitoylation mediates this effect. This activity-sensitive PSD-95 palmitoylation is stoichiometric, as Kyn and APV + CNQX quantitatively

Downloaded from jcb.rupress.org on April 25, 2010

Published July 13, 2009

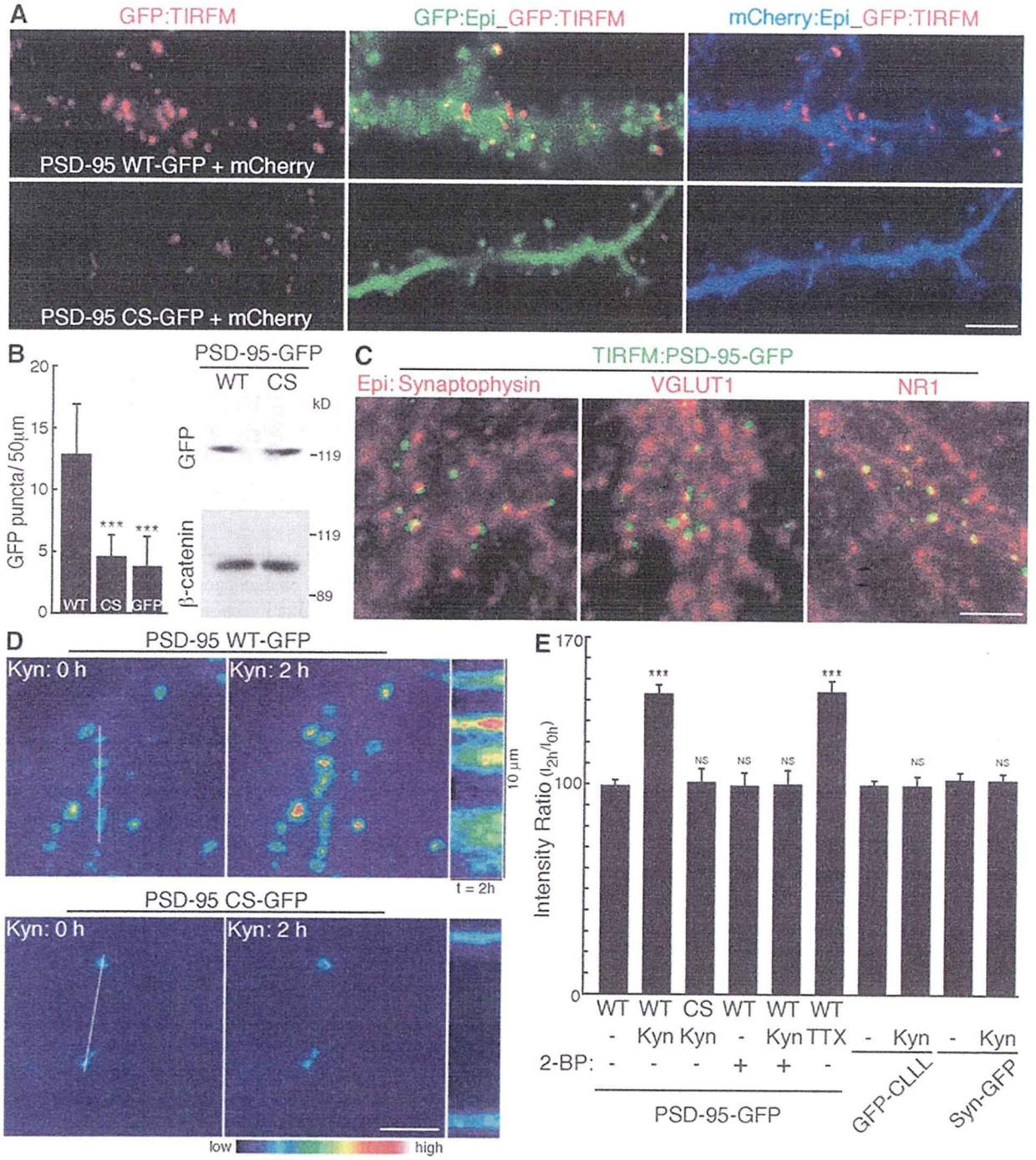

Figure 1. **TIRFM imaging of activity-sensitive PSD-95 palmitoylation.** (A) Compared with epifluorescent microscopy (Epi; green), TIRFM selectively reveals punctae from GFP-tagged PSD-95 (WT) (top; red) but not palmitoylation-deficient PSD-95 (CS) (bottom; red) in cultured hippocampal neurons. To define dendritic morphology, we coexpressed mCherry (Epi; blue). (B) TIRFM preferentially visualizes PSD-95 (WT)–GFP punctae as compared with PSD-95 (CS)–GFP or GFP alone. n = 10 neurons; ***, $P < 0.001$. Comparable expression levels of PSD-95 (WT)– and PSD-95 (CS)–GFP in transfected neuron culture were confirmed. (C) TIRFM tracks synaptic PSD-95. PSD-95 punctae (green) visualized by TIRFM apposed presynaptic synaptophysin and VGLUT1 and overlapped postsynaptic NR1. (D) PSD-95–GFP dynamics were analyzed by time-lapse TIRFM imaging. Inhibition of glutamate receptor activity with 10 mM Kyn increased PSD-95 (WT)–GFP intensity within 2 h. In contrast, the palmitoylation-deficient mutant PSD-95 (CS) did not change. Kymographs represent the changes in the intensity of PSD-95–GFP over 2 h. White lines indicate the regions used for the kymographs. (E) Synaptic accumulation of PSD-95 depends on newly occurring palmitoylation. Fluorescent intensities of PSD-95–GFP (WT and CS), GFP containing a C-terminal prenylation CaaL motif of Rac1 (GFP-CLLL), and synaptophysin-GFP (Syn-GFP) at 2 h after the indicated treatments were quantified. The intensity of PSD-95 (WT)–GFP but not other membrane-targeting proteins significantly increased upon 10 mM Kyn or 2 μM TTX treatment. Coapplication of 100 μM 2-BP with Kyn completely inhibited Kyn-induced increase of PSD-95–GFP intensity. n = 3–8 experiments; ***, $P < 0.001$ compared with control. (B and E) Error bars indicate SD. Bars: (A) 10 μm; (C and D) 5 μm.

Downloaded from jcb.rupress.org on April 25, 2010

Published July 13, 2009

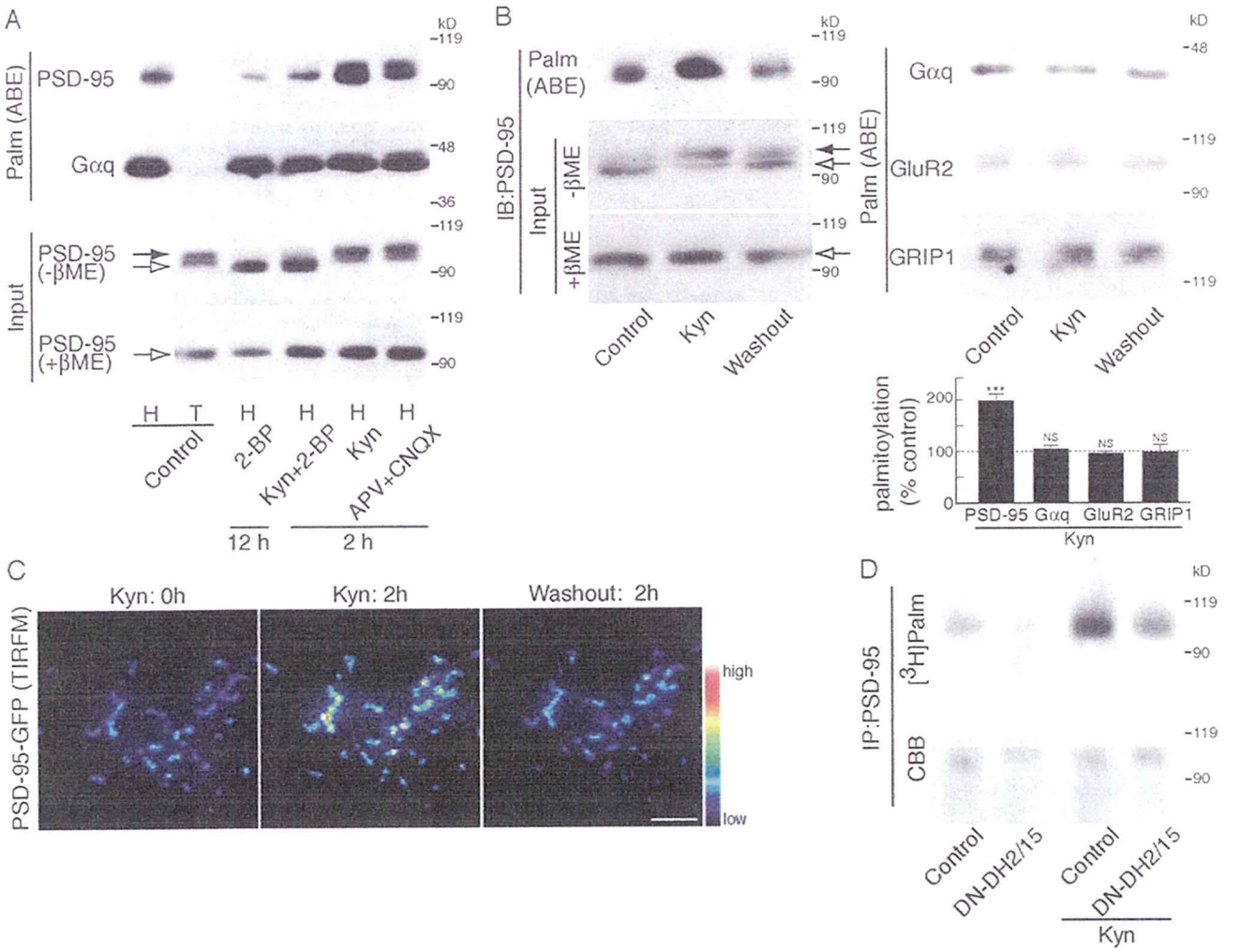

Figure 2. **The DHHC2/15 subfamily of PSD-95 PATs is regulated by synaptic activity.** (A) Activity blockade induces quantitative palmitoylation of PSD-95 but not Gαq. Hydroxylamine (H)-sensitive palmitoylated proteins were purified from treated neurons by the ABE method. The amount of palmitoylated PSD-95 and Gαq was analyzed by Western blotting. T, Tris treatment as a control of hydroxylamine. (B and C) Kyn-induced PSD-95 palmitoylation and synaptic accumulation were reversible upon washing out Kyn. (B) Treatment of hippocampal neurons with Kyn for 2 h enhanced PSD-95 palmitoylation. After washout, PSD-95 palmitoylation level returned to the basal level within 2 h (ABE), with consistent mobility change of PSD-95 (−βME). In contrast, Gαq, GluR2, and GRIP1 palmitoylation did not change upon activity blockade. Kyn-induced palmitoylation changes were quantified. $n = 3$ each; ***, $P < 0.001$. Error bars indicate SD. The dashed line (100%) indicates the normalized control level. IB, immunoblot. (A and B) Closed and open arrows indicate the positions of palmitoylated and nonpalmitoylated PSD-95, respectively. (C) The increased accumulation of PSD-95–GFP upon Kyn treatment returned to the basal level at 2 h after Kyn washout. (D) Cultured hippocampal neurons expressing a DN mutant of the DHHC2 and -15 subfamily (DN-DH2/15) were treated with 3 mCi/ml [^{3}H]palmitate for 2 h in the presence or absence of Kyn. Immunoprecipitated PSD-95 was resolved by SDS-PAGE, followed by fluorography ([^{3}H]palm) and Coomassie staining (CBB). Inhibition of glutamate receptor activity with Kyn greatly enhanced PSD-95 palmitoylation. This enhancement was decreased by DN-DH2/15. IP, immunoprecipitation. Bar, 5 μm.

shifted the PSD-95 band upward (Fig. 2, A and B; Fig. S1 C; and Fig. S2 B). This upward shift reflects palmitoylation, as β-mercaptoethanol (βME), which hydrolyses the palmitoyl thioester, leaves only the lower band (Fig. 2, A and B, bottom). Both the increased PSD-95 palmitoylation and synaptic accumulation were reversible upon washing out of Kyn, indicating that this process is activity sensitive (Fig. 2, B and C).

This activity-sensitive palmitoylation is specific for PSD-95, as Gαq, GluR2, and GRIP1 palmitoylation did not change upon activity blockade (Fig. 2, A and B). Our previous study demonstrated that PSD-95 PATs are DHHC2, -3, -7, and -15, which are phylogenetically divided into two subfamilies, DHHC3/7 and DHHC2/15 (Fukata et al., 2004). Gαq PATs are DHHC3 and -7 (Tsutsumi et al., 2009), and GluR2 PAT is DHHC3 (Fig. S2 C; Hayashi et al., 2005). These substrate selectivities allowed us to ask whether synaptic activity regulates a specific PAT subfamily (i.e., DHHC2/15). We metabolically labeled hippocampal neurons with [^{3}H]palmitic acid for 2 h in the presence or absence of Kyn. We found that Kyn-enhanced PSD-95 palmitoylation was partially blocked by a dominant-negative (DN) mutant, DN-DH2/15, which specifically inhibits the DHHC2/15 subfamily (palmitoylated PSD-95 = 61 ± 15% of Kyn-treated control cells; $P < 0.01$; Fig. 2 D; Fukata et al., 2004). The partial effect of DN-DH2/15 is probably caused by the infection efficiency of DN-DH2/15. Under our conditions, ~50% of neurons were expressing DN-DH2/15,

Downloaded from jcb.rupress.org on April 25, 2010

Published July 13, 2009

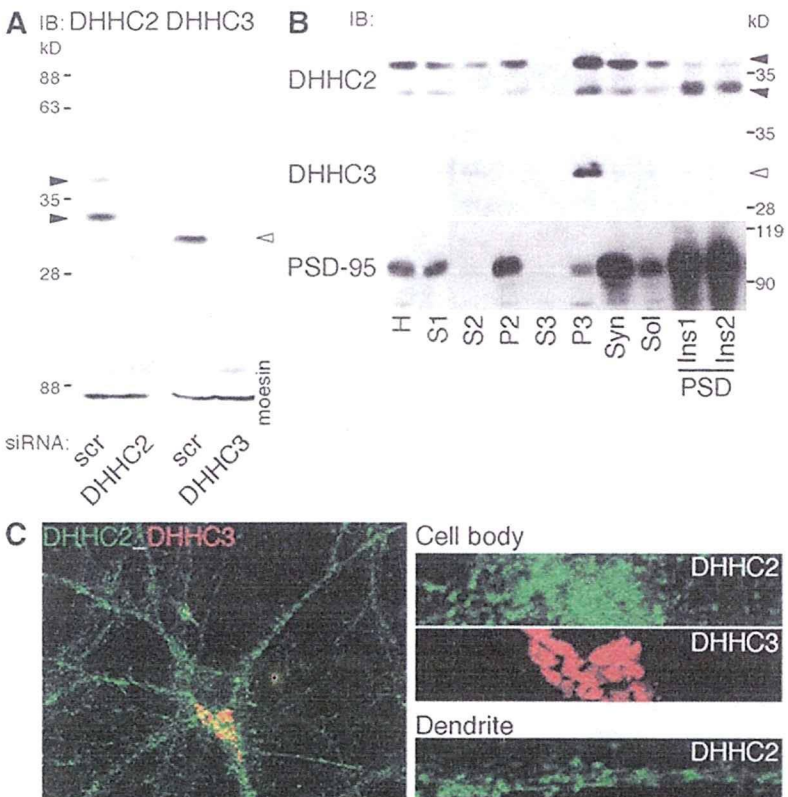

Figure 3. **Differential subcellular distribution of PSD-95 palmitoylating enzymes.** (A) Specificity of antibodies to DHHC2 and -3. The bands detected by anti-DHHC2 (closed arrowheads) and anti-DHHC3 (open arrowhead) antibodies disappeared when protein expression was knocked down by siRNAs. IB, immunoblot; scr, scramble. (B) DHHC2 was enriched in the postsynaptic density (PSD) fractions (Triton X-100–insoluble postsynaptic; closed arrowheads), whereas DHHC3 was detected in only the P3 fraction (open arrowhead). H, homogenate; S, supernatant; P, precipitate; Syn, synaptosome; Sol, Triton X-100 soluble; Ins, Triton X-100–insoluble postsynaptic density fractions. (C) DHHC2 localized in dendrites and the cell body as small vesicular structures, whereas DHHC3 specifically localized at the Golgi apparatus in 18-DIV hippocampal neurons. (D) Effective knockdown of endogenous DHHC2 and -3. Cultured hippocampal neurons were transfected with mCherry-miR RNAi (miDHHC2 and -3) expression vectors at 10 DIV. 18-DIV neurons were stained by DHHC2 or -3 antibody. Note that somatodendritic DHHC2 vesicles and Golgi DHHC3 (arrows) were not stained in mCherry-expressing knocked down neurons (red). Bars: (C [left] and D) 20 µm; (C [right]) 5 µm.

which correlates with the extent of inhibition (~40% inhibition). Although the involvement of other PATs cannot be completely ruled out, our results strongly suggest that the DHHC2/15 subfamily plays a major role in activity-sensitive PSD-95 palmitoylation.

Differential regulation of PSD-95 palmitoylating enzymes in neurons

We next examined the cellular locus for PSD-95 palmitoylation. We focused on DHHC2 and -3, as hippocampal neurons express these PATs but much less DHHC7 and -15 (Fig. S3 A). Immunoblotting with specific antibodies (Fig. 3 A) showed that DHHC2 occurred in the postsynaptic density fraction, whereas DHHC3 was present only in the P3 fraction, which contains Golgi proteins (Fig. 3 B). Consistent with this finding, DHHC3 specifically localizes to the somatic Golgi apparatus (Keller et al., 2004; Tsutsumi et al., 2009), whereas DHHC2 distributes in the dendrites and cell body as small vesicular-like structures (Fig. 3 C). These signals are specific, as the staining completely disappeared in the validated knockdown vector–transfected neuron (Fig. 3 D).

DHHC2 or -3 knockdown by microRNA (miRNA; miDHHCs) greatly reduced the number of PSD-95 punctae (Fig. 4, A and B). Importantly, knockdown of DHHC2 but not DHHC3 prevented Kyn- or TTX-induced increase of endogenous PSD-95 accumulation at synaptic sites (Fig. 4, A, C and D) and Kyn-induced augmentation of PSD-95–GFP accumulation (Fig. 5 and Video 3). The inhibitory effect of miDHHC2 was rescued by miDHHC2-resistant WT DHHC2 (WT) but not by PAT-inactive DHHC2 (CS) (Fig. 5 and Fig. S4 C). These results indicate that DHHC3 localizes to the Golgi apparatus and mediates constitutive palmitoylation of various substrates, including PSD-95, Gαq, and $GABA_A$ receptor-γ subunit (Fukata et al., 2004; Keller et al., 2004; Tsutsumi et al., 2009). In contrast, dendritic DHHC2 mediates activity-sensitive PSD-95 palmitoylation.

Dendritic DHHC2 translocates near postsynaptic sites upon activity blockade

We next investigated whether DHHC2 PAT activity, monitored by autopalmitoylation (Fukata et al., 2004), was regulated by synaptic activity. Whereas PSD-95 palmitoylation increased

Downloaded from jcb.rupress.org on April 25, 2010

Published July 13, 2009

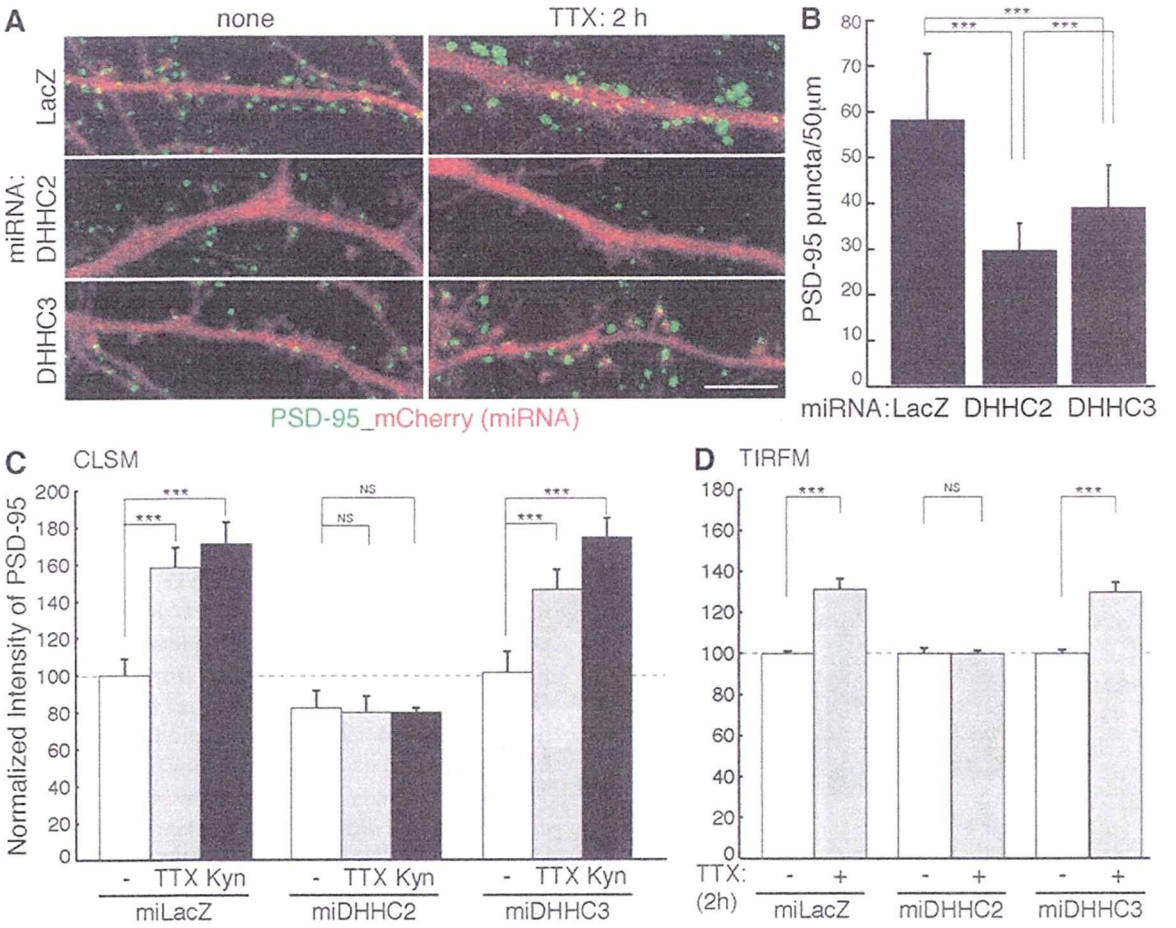

Figure 4. **DHHC2 and -3 are differently involved in PSD-95 trafficking.** (A and B) In the DHHC2 or -3 knocked down neurons (labeled with mCherry), the number of native PSD-95 puncta (green) was significantly decreased. *n* = 5 neurons; ***, P < 0.001. (C and D) Knockdown of DHHC2 but not DHHC3 prevented TTX- or Kyn-induced augmentation of endogenous PSD-95 accumulation. Dashed lines (100%) indicate the normalized control level. ***, P < 0.001. (C) Analyzed by confocal laser-scanning microscopy (CLSM). *n* = 10–15 neurons. (D) Analyzed by TIRFM. *n* = 5 neurons. miLacZ is a control miRNA targeting LacZ (β-galactosidase). (B–D) Error bars indicate SD. Bar, 5 µm.

upon TTX or Kyn treatment, autopalmitoylation of DHHC2 and -3 did not change (Fig. 6 A), suggesting that DHHC2 activity may remain constant. We then investigated whether DHHC2 localization is regulated by synaptic activity. TIRFM imaging revealed that more DHHC2 was recruited near the membrane upon Kyn or TTX treatment (Fig. 6, B and C; and Video 4), where PSD-95 localized (Fig. S4 A). This translocation was activity sensitive as it was reversible upon washing out of Kyn (Fig. 6 D). Furthermore, we found that Kyn or TTX steadily induced colocalization of endogenous DHHC2 with PSD-95 over 48 h (Fig. 6, E and F), whereas DHHC3 remained at the Golgi apparatus (Fig. S4 B).

Activity-sensitive PSD-95 palmitoylation by DHHC2 is necessary for homeostatic increase of AMPARs

Because PSD-95 anchors AMPARs at the postsynaptic sites through interaction with stargazin and related transmembrane AMPAR regulatory proteins (TARPs; Chen et al., 2000; Nicoll et al., 2006), we investigated changes in synaptic AMPARs upon activity blockade. We took advantage of the pHluorin-tagged GluR1 (pH-GluR1) subunit (Ashby et al., 2004; Yudowski et al., 2007) and TIRFM imaging to monitor specifically surface-expressed GluR1 (Video 5). pH-GluR1 punctate intensity was invariant over 12 h (Fig. 7, A and D; and Video 6). In contrast, TTX treatment gradually and continually increased pH-GluR1 intensity (Fig. 7, B and D; and Video 7). By post hoc immunostaining with PSD-95, we found that pH-GluR1 punctae by TIRFM completely overlapped PSD-95 clusters (Fig. 7 C). Furthermore, knockdown of DHHC2 or PSD-95 completely blocked this increase of pH-GluR1 intensity (Fig. 7, D and E). The effect of DHHC2 knockdown was rescued by miDHHC2-resistant WT DHHC2 (WT) but not by PAT-inactive DHHC2 (CS) (Fig. 7 E and Video 8). The effect of PSD-95 knockdown was rescued by short hairpin RNA–resistant WT PSD-95 (WT) but not by palmitoylation-deficient PSD-95 (CS) (Fig. 7 E, Fig. S4 D, and Video 9). We also found that knockdown of DHHC2 or PSD-95 similarly inhibited Kyn-induced increase of pH-GluR1 (Fig. 7 D). pH-GluR2, endogenous GluR1, GluR2, and stargazin-like TARPs but neither NR2A NMDA receptor nor VGLUT1 showed an increase similar to that of pH-GluR1 (Fig. S5).

Downloaded from jcb.rupress.org on April 25, 2010

Published July 13, 2009

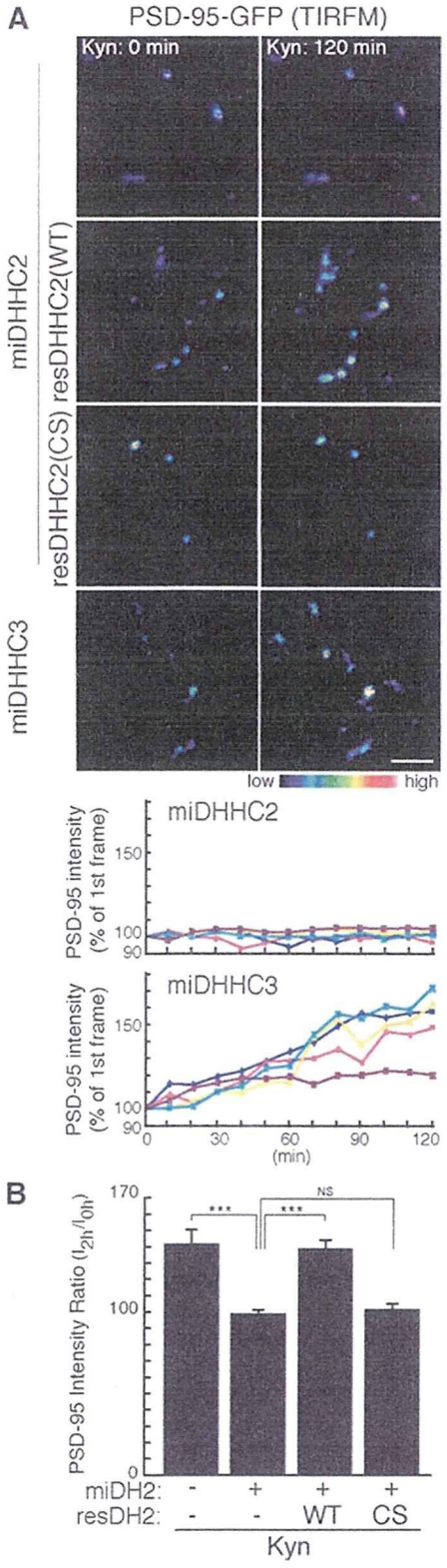

Figure 5. **DHHC2 is essential for activity-sensitive PSD-95 palmitoylation.** (A and B) DHHC2 but not DHHC3 mediates palmitoylation of PSD-95 upon activity blockade. Knockdown of DHHC2 but not DHHC3 inhibited Kyn-induced PSD-95–GFP recruitment at the synaptic membrane. miDHHC2-resistant DHHC2 (WT) but not PAT-inactive DHHC2 (CS) rescued Kyn-induced PSD-95 accumulation. (A) TIRFM intensity of representative five punctae from a neuron was plotted with time. (B) $n = 3$ each; ***, $P < 0.001$. Error bars indicate SD. Bar, 5 µm.

Similar inhibitory effects of DHHC2 or PSD-95 knockdown were observed for endogenous GluR1, GluR2, and TARPs (Fig. S5 G). These results indicate that activity-sensitive PSD-95 palmitoylation by DHHC2 mediates the homeostatic increase of AMPARs.

Discussion

By contrasting two representative PSD-95 palmitoylating enzymes, this study is the first to define differential regulation of DHHC-type palmitoylating enzymes. DHHC3 stably localizes at the Golgi apparatus and constitutively palmitoylates numerous substrates, including Gα, GluR2, and PSD-95. In contrast, dendritically localized DHHC2 senses changes in synaptic activity and rapidly translocates near postsynaptic membranes. Synaptically translocated DHHC2 induces rapid, specific, and stoichiometric palmitoylation and synaptic accumulation of PSD-95 and thereby AMPAR recruitment at postsynaptic sites. Thus, activity-sensitive DHHC2 translocation marks sites for AMPAR accumulation through compartmentalized PSD-95 palmitoylation. Complementing these findings, previous works showed that the *Drosophila melanogaster* DHHC17/HIP14 homologue localizes primarily to presynaptic terminals and acts on presynaptic Cys string protein and SNAP-25 (Ohyama et al., 2007; Stowers and Isacoff, 2007). The DHHC family members show distinctive subcellular distributions and different intracellular dynamics upon physiological stimuli. These distinctive properties provide mechanisms for specific control of protein palmitoylation by the large family of DHHC proteins.

Recent fluorescence recovery after photobleaching and photoconversion analyses revealed that several palmitoylated proteins such as Harvey Ras/neuroblastoma Ras (Rocks et al., 2005), Gαo (Chisari et al., 2007), and Gαq (Tsutsumi et al., 2009) rapidly shuttle between the plasma membrane and the Golgi apparatus. This constitutive shuttling comprises four steps: (1) palmitoylation by the Golgi-resident DHHC proteins, (2) trafficking to the plasma membrane, (3) depalmitoylation by a putative PPT and rapid cytosolic diffusion, and (4) transient trapping at the Golgi for repalmitoylation (Fig. 8 A; Rocks et al., 2006; Tsutsumi et al., 2009). In neurons, where the Golgi apparatus is segregated from the axon and dendrites, we suggest that Golgi-localized DHHC3 mediates the constitutive palmitoylation of PSD-95 at the cell body. In dendrites, PSD-95 depalmitoylated at the postsynaptic membrane diffuses from dendritic spine to shaft, is repalmitoylated on DHHC2-positive vesicles, and is redirected to postsynaptic membranes (Fig. 8 B). When synaptic activity is blocked, DHHC2 vesicles translocate from dendritic shafts to sites near the postsynaptic membrane. This allows DHHC2 to repalmitoylate PSD-95 in the spine (Fig. 8 C). Thus, mobile DHHC2 induces a local increase of PSD-95 palmitoylation, which leads to AMPAR recruitment. We propose that extracellular signals translocate specific DHHC PATs and create a new route for substrate shuttling between loci of palmitoylation and depalmitoylation, leading to efficient and precise substrate targeting. Such a compartmentalized regulatory mechanism of DHHC PATs may contribute to spatiotemporal

Downloaded from jcb.rupress.org on April 25, 2010

Published July 13, 2009

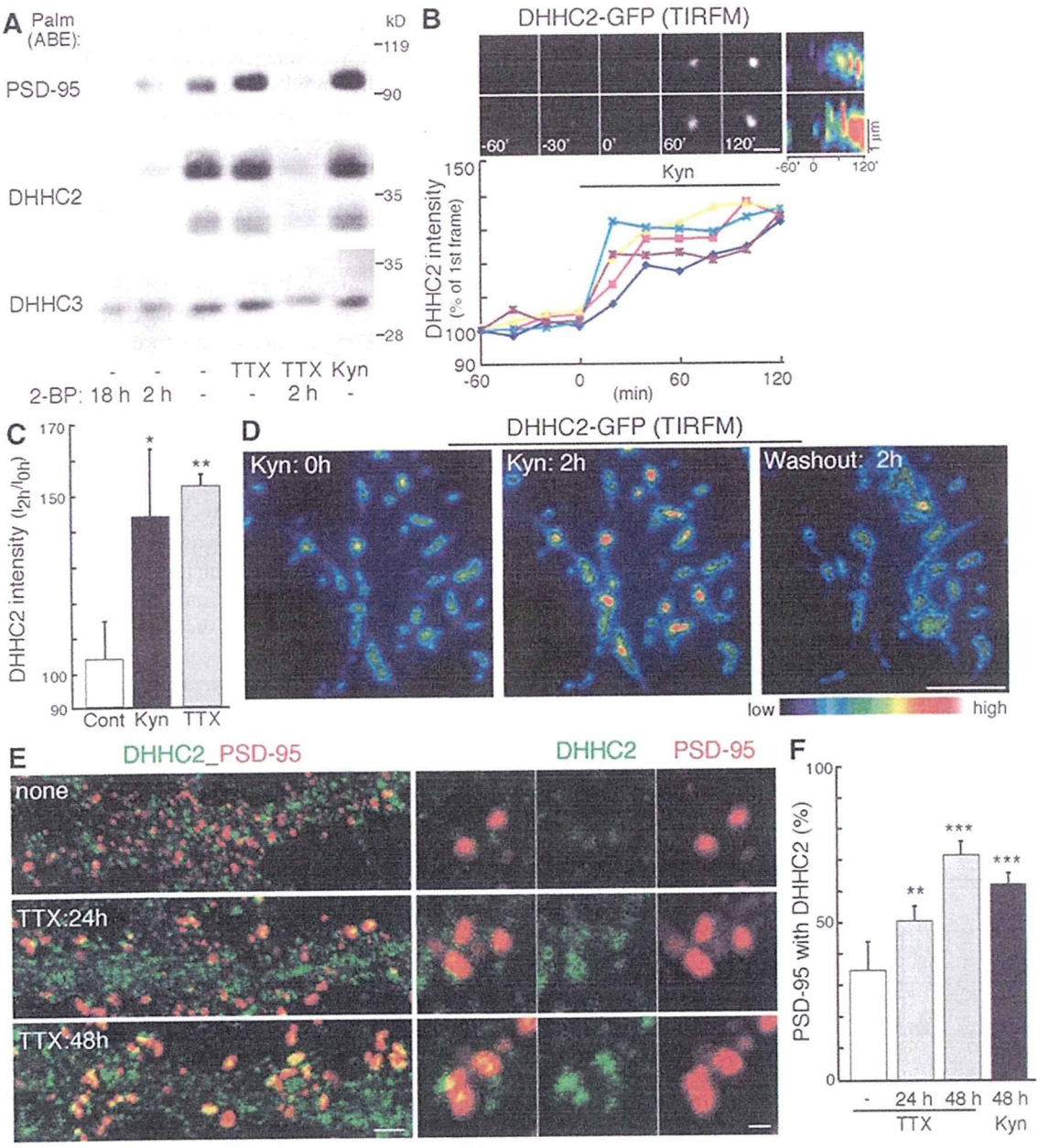

Figure 6. **Activity-sensitive synaptic translocation of DHHC2.** (A) No change in DHHC autopalmitoylation (detected by the ABE method) was seen upon activity blockade (TTX or Kyn) of hippocampal neurons, suggesting that DHHC activity remains constant. (B and C) TIRFM imaging revealed that treatment with Kyn or TTX translocated DHHC2-GFP near the plasma membrane. $n = 3$; *, $P < 0.05$; **, $P < 0.01$ compared with control. Kymographs (pseudocolor) represent the changes in the intensity of DHHC2-GFP over time. (D) The translocation of DHHC2-GFP induced by Kyn treatment was reversible upon washing out Kyn. (E and F) Colocalization of endogenous DHHC2 with PSD-95 steadily increased over prolonged TTX or Kyn treatment. (F) $n = 5$–7 each; **, $P < 0.01$; ***, $P < 0.001$. (C and F) Error bars indicate SD. Bars: (B) 2 μm; (D) 5 μm; (E [left]) 3 μm; (E [right]) 1 μm.

regulation of signaling molecules in polarized neurons, epithelial cells, and migrating cells.

This study monitors intracellular dynamics of palmitoylated proteins by taking advantage of time-lapse TIRFM, which visualizes membrane-associated proteins with exquisite sensitivity. This approach allowed us to follow dynamic changes in membrane-associated PSD-95–GFP over time in individual neurons. However, one may ask whether endogenous PSD-95 shows similar dynamics and whether TIRFM visualizes a limited set of synaptic contacts. The TIRFM limitation was supplemented with epifluorescent and confocal microscopic analyses on endogenous PSD-95. Also, our biohemical approaches, including metabolic labeling and the ABE method, showed that blocking synaptic activity quantitatively increases endogenously palmitoylated PSD-95, supporting the specificity of TIRFM imaging as a method for monitoring palmitoylated proteins in living cells.

A previous study reported that glutamate receptor activation accelerates depalmitoylation of PSD-95, dissociates PSD-95 from postsynaptic sites, and causes AMPAR endocytosis

Downloaded from jcb.rupress.org on April 25, 2010

Published July 13, 2009

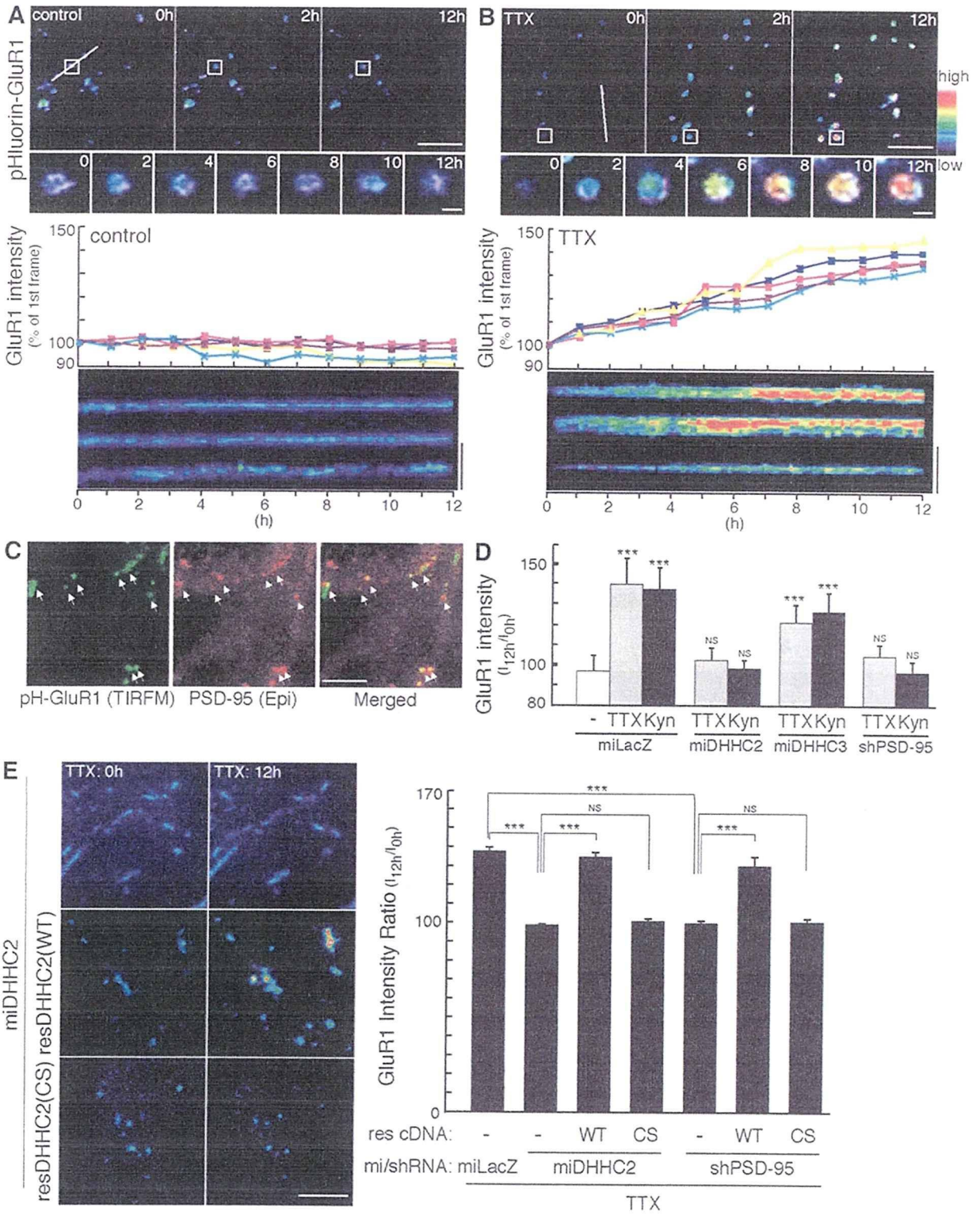

Figure 7. **Essential role of DHHC2-mediated PSD-95 palmitoylation in AMPAR homeostasis.** (A and B) Upon 2 µM TTX treatment, TIRFM intensity of pH-GluR1 punctae gradually and continually increased over a 12-h observation. Fluorescence intensity was displayed in pseudocolor and was plotted with time. Kymographs represent the changes in the intensity of pH-GluR1. White lines indicate the regions used for the kymographs. Insets are magnified in the middle panels. (C) Post hoc immunostaining with PSD-95 showed that all GluR1 punctae by TIRFM overlapped synaptic PSD-95 clusters (arrows). (D) Quantification of fluorescent intensities of pH-GluR1 by TIRFM at 12 h after TTX or Kyn treatment. Knockdown of DHHC2 or PSD-95 completely inhibited the homeostatic increase of surface GluR1. $n = 3$ each; ***, $P < 0.001$ compared with nontreated control. miLacZ is a control miRNA targeting LacZ. (E) The inhibitory effect of DHHC2 knockdown was rescued by miDHHC2-resistant DHHC2 (WT) but not by PAT-inactive DHHC2 (CS). Furthermore, the inhibitory effect of PSD-95 knockdown was rescued by short hairpin RNA–resistant PSD-95 (WT) but not by palmitoylation-deficient PSD-95 (CS). $n = 3$ for each; ***, $P < 0.001$. (D and E) Error bars indicate SD. Bars: (A and B [top] and C) 10 µm; (A and B [insets]) 0.5 µm; (A and B [bottom] and E) 5 µm.

Downloaded from jcb.rupress.org on April 25, 2010

Published July 13, 2009

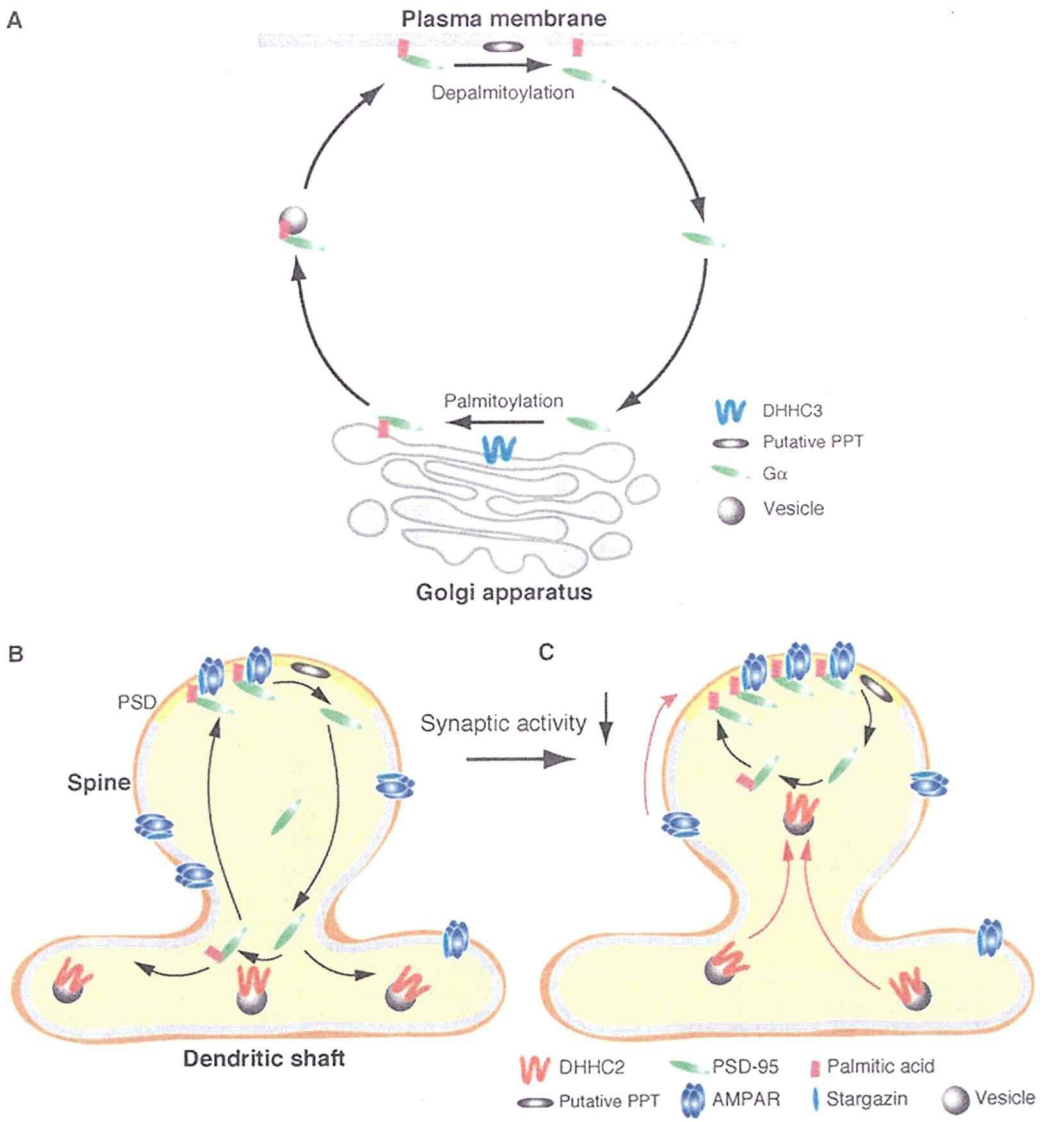

Figure 8. **Model for compartmentalized synaptic palmitoylation of PSD-95 by mobile DHHC2.** (A) Certain palmitoylated proteins such as the Gα subunit shuttle between the plasma membrane and the Golgi in nonpolarized cells. Golgi-resident DHHC3 and a putative PPT at the plasma membrane can mediate this constitutive shuttling. In neurons, DHHC3 localizes at the Golgi apparatus and mediates constitutive palmitoylation of various substrates, including Gα and PSD-95. (B and C) PSD-95 shuttling in dendrites. (B) A dynamic equilibrium exists between palmitoylated postsynaptic PSD-95 and nonpalmitoylated cytosolic PSD-95. Depalmitoylated PSD-95 diffuses into the spine and dendritic shaft. DHHC2 PAT mainly localizes in dendritic shafts on vesicles and mediates dendritic PSD-95 palmitoylation. PSD, postsynaptic density. (C) When synaptic activity is blocked, DHHC2 vesicles move into spines. This translocated DHHC2 palmitoylates spinous PSD-95; the increased postsynaptic PSD-95 thereby contributes to AMPAR homeostasis.

(El-Husseini et al., 2002). This sequence suggested that a PPT serves as the regulatory trigger. In contrast, our work demonstrates that activity blockade–induced PSD-95 palmitoylation up-regulates synaptic AMPARs. Thus, the palmitoylation/depalmitoylation cycle of PSD-95 bidirectionally contributes to AMPAR homeostasis (O'Brien et al., 1998; Turrigiano et al., 1998; Stellwagen and Malenka, 2006). By analogy, β-adrenergic receptor activation markedly accelerates depalmitoylation of Gαs, shifts Gαs to the cytoplasm, and down-regulates β-adrenergic receptor–mediated signaling (Wedegaertner and Bourne, 1994). Collectively, these studies suggest that palmitate cycling may generally mediate homeostasis of receptor-mediated signaling.

Recently, it was shown that both PSD-95 and PSD-93 play important roles in AMPAR trafficking (Elias et al., 2006). In this study, we found that knockdown of PSD-95 alone completely blocks the TTX- or Kyn-induced recruitment of AMPARs to the synapse. One may wonder why knockdown of PSD-95 alone completely blocks the TTX- or Kyn-induced AMPAR recruitment. We quantified expression levels of PSD-95 and PSD-93 in our cultured 18-d in vitro (DIV) hippocampal neurons by quantitative Western blotting. We found that PSD-95 expresses about eight times as much as PSD-93 (Fig. S3 B). Furthermore, we found that PSD-93–β, one of the major PSD-93 isoforms (Firestein et al., 2000; Parker et al., 2004), is specifically palmitoylated by the DHHC3 and -7 subfamily but not

Downloaded from jcb.rupress.org on April 25, 2010

Published July 13, 2009

by the DHHC2 and -15 subfamily (Fig. S3 C), indicating that PSD-93–β palmitoylation is differently regulated from PSD-95 palmitoylation. Furthermore, it was reported that palmitoylation of PSD-93–α and PSD-93–β is not necessary for their postsynaptic targeting (Firestein et al., 2000). Collectively, we conclude that PSD-95 plays a major role in DHHC2-mediated AMPAR recruitment upon activity blockade.

Global proteomic studies indicate that palmitoylation represents a common posttranslational modification (Roth et al., 2006; Kang et al., 2008). Importantly, many palmitoylated proteins are key signaling molecules that subserve physiological processes. Furthermore, mutations of DHHC family members have been detected in cancers (Oyama et al., 2000; Mansilla et al., 2007; Yamamoto et al., 2007) and neurological disorders (Mukai et al., 2004, 2008; Mansouri et al., 2005; Yanai et al., 2006; Raymond et al., 2007). Elucidation of molecular mechanisms for palmitoylation lays a foundation to understand its role in physiological and pathological conditions. Because DHHC enzymes show substrate specificity, DHHC PATs represent exciting therapeutic targets. Our experiments of differential partitioning and regulation on DHHC PATs should serve as a prototype for understanding how dynamic protein palmitoylation is regulated in divergent signaling environments.

Materials and methods

Materials

The following antibodies were used: rabbit polyclonal antibodies to DHHC3/GODZ (Abcam), Gαq (Santa Cruz Biotechnology, Inc.), GluR1 (EMD; Millipore), GRIP1 (Millipore), PSD-93 (Millipore), and stargazin/TARP (Millipore); a guinea pig polyclonal antibody to VGLUT1 (Millipore); and mouse monoclonal antibodies to β-catenin (BD), GluR2 (Millipore), HA (Covance), NMDAR1 (Millipore), PSD-95 (Thermo Fisher Scientific), and synaptophysin (Sigma-Aldrich). Anti–PSD-93 antibody was raised against (aa 336–379) and detected all isoforms of PSD-93. Rabbit polyclonal antibodies to GFP, PSD-95, and moesin were raised against GFP (aa 1–239), GST–PSD-95 (aa 1–434), and GST-moesin (aa 307–577), respectively, and affinity purified. A mouse monoclonal antibody to DHHC2 was raised by a baculovirus display method, which is useful for the production of antibodies against membrane proteins (Masuda et al., 2003; Saitoh et al., 2007). The following reagents were used: Kyn and APV (Tocris); TTX (Nacalai Tesque, Inc.); CNQX and CHX (Sigma-Aldrich); and 2-bromohexadecanoic acid (2-BP; Fluka).

For knockdown experiments in HEK293 cells, siRNAs from QIAGEN were used: scramble (Allstars negative control), siDHHC2, and siDHHC3. siRNA and plasmid-based miRNA for DHHCs were validated by two methods: (1) reduced expression of exogenously expressed DHHC proteins in HEK293 cells (Western blotting) and (2) down-regulation of endogenous mRNAs in HEK293 cells (quantitative real-time PCR).

Cloning and plasmid constructions

The rat cDNAs of synaptophysin (GenBank/EMBL/DDBJ accession no. NM_012664), DHHC2 (GenBank/EMBL/DDBJ accession no. AF228917), DHHC3 (GenBank/EMBL/DDBJ accession no. NM_001039014), DHHC7 (GenBank/EMBL/DDBJ accession no. NM_133394), and DHHC15 (GenBank/EMBL/DDBJ accession no. AY886531) were cloned from rat brain total RNA by RT-PCR. Synaptophysin was subcloned into pCAGGS-GFP, and DHHC2, -3, -7, and -15 were subcloned into pEF-Bos-HA and pcDNA3.1. The mutant rat DHHC2(C156S) was generated by using site-directed mutagenesis. pGW1-rat PSD-95–GFP, pGW1-rat PSD-93–β-GFP and pEF-Bos-HA-mouse DHHC constructs were described previously (El-Husseini et al., 2002; Fukata et al., 2004; Parker et al., 2004). pGW1–PSD-95–HA was constructed by replacing a GFP fragment with a synthetic DNA fragment encoding HA. pEGFP-C1-Rac1-CLLL was described previously (Nakagawa et al., 2001). To obtain the antigen for antibody production, DHHC2 was subcloned into the pcDNA-His-Flag vector. His-Flag–tagged DHHC2 was then subcloned into pAcYM1 for baculovirus production. DHHC2 was also subcloned into pGW1-GFP. To obtain Thy1/pH-GluR1, we first inserted pHluorin between residues 21 and 22 of rat GluR1 (Tomita et al., 2004) and subcloned pH-GluR1 into a Thy1 expression cassette. pCAGGS–pH-GluR2 was made by inserting pHluorin between residues 23 and 24 of mouse GluR2 (Fukata et al., 2005). cDNA of NR2A-GFP (Luo et al., 2002) was subcloned into the pCAGGS vector.

In cultured hippocampal neurons, DHHC2 and -3 were knocked down by the miR-RNAi system (Invitrogen). We used BLOCK-iT RNAi Designer (Invitrogen) to select the targeting sequences, and the following targeting sequences were used (targeting both rat and human sequences): miDHHC2, 5′-GGTGAACAATTGTGTTGGATT-3′ (alternative sequence, 5′-TGTGCATAGTGTCCATGGAAA-3′; both sequences yielded similar results); miDHHC3, 5′-TGAGACGGGAATAGAACAATT-3′; and miLacZ, 5′-GACTACACAAATCAGCGATTT-3′ (as a negative control). After subcloning these oligonucleotides into pcDNA6.2-EmGFP-miR (Invitrogen), EmGFP was replaced with mCherry, and the pre-miRNA expression cassette of pcDNA6.2-mCherry-miR (or pcDNA6.2-EmGFP-miR) was transferred to the pCAGGS vector with a β-actin promoter. PSD-95 was knocked down as described previously (Elias et al., 2006), replacing GFP of pLLox3.7 (American Type Culture Collection) with mCherry. DHHC2 (on pEF-Bos-HA-rat DHHC2) and PSD-95 (on pGW1-rat PSD-95–HA) rescue constructs that have two and four different nucleotides in the target sequences were generated by using site-directed mutagenesis (DHHC2, 5′-GGTGAACAACTGCGTTGGATT-3′; PSD-95, 5′-TCACAATAATAGCCCAGTATA-3′; changed nucleotides are underlined). All PCR products were analyzed by DNA sequencing.

pcDNAI-Gαq-GFP was provided by C.A. Berlot (Weis Center for Research, Danville, PA; Hughes et al., 2001). The cDNAs of pHluorin and mCherry were provided by J.E. Rothman (Columbia University, New York, NY; Miesenbock et al., 1998) and R.Y. Tsien (University of California, San Diego, La Jolla, CA; Shaner et al., 2005), respectively. cDNAs of rat GluR1, NR2A-GFP, and pEGFP-C1-Rac1-CLLL were gifts from R. Huganir (Johns Hopkins University, Baltimore, MD), S. Vicini (Georgetown University School of Medicine, Washington, DC), and K. Kaibuchi (Nagoya University, Showa-Ku, Nagoya, Japan), respectively. Thy1 expression cassette was provided by D. Monard (Friedrich Miescher Institute, Basel, Switzerland; Luthi et al., 1997).

Time-lapse imaging with TIRFM

Hippocampal neuron cultures were prepared from rat embryonic day 18–19 embryos. All animal experiments described herein were reviewed and approved by the ethical committee in our institutes and were performed according to the institutional guidelines concerning the care and handling of experimental animals. Neurons were seeded at a density of 2.5×10^5 cells per 3.5-cm glass-based dish (Iwaki) in neurobasal medium (Invitrogen) supplemented with B-27 supplement (Invitrogen) and 2 mM Glutamax (Invitrogen). 8–10-DIV neurons were transfected by Lipofectamine 2000 (Invitrogen) and observed (18–21 DIV) at 37°C in a microincubator (MI-IBC-IF; Olympus) with an inverted microscope (IX81; Olympus) equipped with a Plan-Apochromat 100× NA 1.45 oil TIRFM objective lens, an ImageEM charge-coupled device (CCD) camera (C9100-13; Hamamatsu Photonics) and Meta Imaging software version 7.1 (MDS Analytical Technologies). A 488-nm laser was used as a light source. Time-lapse images were taken every 10 min with a laser-based zero drift autofocusing system (IX81-ZDC; Olympus), which adjusts the focal plane to the initial focal plane just before each imaging frame. The video files (QuickTime Movie) were produced with ImageReady 2.0 (Adobe Systems, Inc.). To quantitate changes in PSD-95–GFP, DHHC2-GFP, or pH-GluR1 intensity by TIRFM, we randomly chose fields, and the punctae (>1.25 µm in diameter) were quantitated in every frame. Fluorescent intensities from TIRF images were analyzed using MetaMorph software version 7.1 (MDS Analytical Technologies). The ratios of intensities at 0–120 min (for PSD-95 and DHHC2) or 0–12 h (for GluR1) in 50–100 randomly selected punctae (three to eight independent experiments) are shown. Kymographs were produced using Meta Imaging software version 7.1.

Immunofluorescence analysis of hippocampal neuron culture

Cultured hippocampal neurons (5×10^4 cells) were seeded onto 12-mm coverslips in 24-well dishes. 18–28-DIV neurons were fixed with 4% paraformaldehyde/120 mM sucrose/100 mM Hepes, pH 7.4, at room temperature for 10 min, permeabilized with 0.1% Triton X-100 for 10 min, and blocked with PBS containing 10 mg/ml BSA for 10 min on ice. For staining of DHHC2 and VGLUT1, neurons were fixed with methanol for 10 min at −30°C. For mouse anti-DHHC2 antibody, Alexa Fluor 488–conjugated anti–mouse IgG_1 subtype specific (Invitrogen) was used as a secondary antibody. For surface GluR1 and GluR2 staining, GluR1 and GluR2 receptors were "live" labeled with an antibody to an extracellular

Downloaded from jcb.rupress.org on April 25, 2010

Published July 13, 2009

epitope of GluR1 (EMD) or GluR2 (Millipore) by incubating neurons in conditioned medium for 15 min at 37°C. Neurons were then fixed with 2% paraformaldehyde for 20 min and blocked as described above. Surface GluR1 and GluR2 were visualized with Alexa Fluor 488–conjugated secondary antibody. Fluorescent images were taken with a confocal laser-scanning microscopy system (LSM5 Exciter; Carl Zeiss, Inc.) equipped with a Plan-Apochromat 63× NA 1.40 oil immersion objective lens. For knockdown experiments, 8–12-DIV neurons were transfected with pCAGGS-mCherry-miR vectors by Lipofectamine 2000. At 8–10 d after transfection, neurons were stained with anti-DHHC2, DHHC3, PSD-95, GluR1, GluR2, and stargazin/TARP antibodies. To quantitate the intensity of PSD-95 clusters and surface GluR1, surface GluR2, or TARP clusters (costained with PSD-95), we randomly chose 10–15 fields from two independent neuronal cultures (on treated and age-matched sister control cultures) and analyzed the three largest caliber proximal dendrites (20 µm long; at least 400 clusters). We measured the mean intensities of individual clusters (>1 µm diameter) along these dendritic segments. Microscope control and all image analyses were performed with ZEN software (Carl Zeiss, Inc.). Brightness and contrast adjustments were applied to the whole image using Photoshop CS3 (Adobe Systems, Inc.). For some experiments, immunolabeled samples were observed by TIRFM and epifluorescent microscopy.

ABE method

The ABE method was performed as previously described (Roth et al., 2006; Kang et al., 2008) and modified for cultured neurons. After treating 18–28-DIV hippocampal neurons (5×10^5 cells/6-well dish) with the indicated antagonists or inhibitors, neurons were washed with PBS containing 10 mM *N*-ethyl-maleimide (NEM) twice and solubilized with 0.1 ml of lysis buffer (LB; 50 mM Tris-HCl, pH 7.5, 5 mM EDTA, and 50 mM NaCl) containing 2% SDS and 10 mM NEM. After 15 min of extraction, LB with 2% Triton X-100 and 10 mM NEM was added to a final volume of 1 ml and incubated for 1 h at 4°C. After centrifugation at 20,000 *g* for 10 min, the supernatants were precipitated by the chloroform-methanol (CM) method (Wessel and Flugge, 1984). Precipitated protein was solubilized in 0.2 ml SB (50 mM Tris-HCl, pH 7.5, 5 mM EDTA, and 4% SDS) containing 10 mM NEM at 37°C for 10 min. The protein was diluted into 0.8 ml LB with 0.2% Triton X-100 and 1 mM NEM and incubated overnight at 4°C. NEM was removed by three sequential CM precipitations. Precipitated protein was solubilized in 0.2 ml of buffer SB, and then 0.8 ml HB (1 M hydroxylamine, pH 7.5, 150 mM NaCl, 0.2% Triton X-100, and 1 mM biotin-HPDP) or buffer TB (1 M Tris-HCl, pH 7.5, 150 mM NaCl, 0.2% Triton X-100, and 1 mM biotin-HPDP) was added. The mixture was incubated for 1 h at room temperature and subjected to CM precipitation. The precipitated protein was dissolved in 0.2 ml SB, diluted into 0.8 ml LB containing 150 mM NaCl, 0.2% Triton X-100, and 200 µM biotin-HPDP, and incubated for 1 h at room temperature. Free biotin-HPDP was removed by CM precipitation. The precipitated protein was solubilized in 100 µl of buffer UB (50 mM Tris-HCl, pH 7.5, 5 mM EDTA, and 2% SDS) and diluted in 900 µl LB with 0.2% Triton X-100. After brief centrifugation, the supernatant was incubated with 30 µl neutravidin-agarose (Thermo Fisher Scientific) for 1 h at 4°C. After washing the beads with LB containing 0.1% SDS and 0.2% Triton X-100, bound proteins were suspended in SDS-PAGE sample buffer (62.5 mM Tris-HCl, pH 6.8, 10% glycerol, 2% SDS, and 0.001% bromophenol blue) with 10 mM DTT (without βME; −βME) and boiled at 90°C for 2 min. To see the palmitoylation-dependent mobility shift of PSD-95, the cell lysate was treated similarly (−βME). To reduce the sample completely, the lysate was separately treated with SDS-PAGE sample buffer with 2% βME at 100°C for 5 min (+βME). Samples were subjected to SDS-PAGE and Western blotting with the indicated antibodies.

In vivo palmitate labeling

Hippocampal neurons were infected with Semliki forest virus to express GFP or GFP-tagged DN DHHC2/15 (Fukata et al., 2004). At 24 h after infection, cells were labeled for 2 h in neurobasal media containing 3 mCi/ml [^{3}H]palmitic acid (PerkinElmer) either in the presence or absence of 10 mM Kyn. Labeled cells were washed with PBS and resuspended in 0.15 ml LB A (20 mM Tris-HCl, pH 7.5, 1 mM EDTA, 100 mM NaCl, and 1% SDS). After 5 min of extraction, 1% Triton X-100 was added to a final volume of 1.5 ml. After centrifugation at 20,000 *g* for 10 min, the supernatants were incubated with rabbit anti–PSD-95 antibody for 1 h and then incubated for 1 h with 30 µl protein A–Sepharose (GE Healthcare) at 4°C. Immunoprecipitates were washed three times with buffer containing 20 mM Tris-HCl, pH 7.4, 1 mM EDTA, 100 mM NaCl, and 1% Triton X-100. Immunoprecipitated PSD-95 was suspended in SDS sample buffer. For fluorography, protein samples were separated by SDS-PAGE. Gels were treated with Amplify (GE Healthcare) for 30 min, dried under vacuum, and exposed to Biomax MS (Kodak) at −80°C for 2 wk. After autoradiography, the bands were scanned and analyzed with National Institutes of Health software.

Transfected HEK293 cells were preincubated for 30 min in serum-free DME with 5 mg/ml fatty acid–free BSA (Sigma-Aldrich). Cells were then labeled with 0.25 mCi/ml [^{3}H]palmitic acid for 4 h in the preincubation medium. Cells were washed with PBS and scraped with SDS-PAGE sample buffer with 10 mM DTT. The cell lysate was resolved by SDS-PAGE, followed by fluorography (36-h exposure) and Western blotting.

In situ hybridization

In situ hybridization on 7-µm paraffin-embedded 3-wk-old rat brain sections (Genostaff) was performed by using digoxigenin-labeled RNA probes. cDNAs of mouse DHHC2 (nt 1–1,098 from initiating ATG), rat DHHC3 (nt 1–900), rat DHHC7 (nt 1–927), rat DHHC15 (nt 1–1,014), and rat PSD-95 (nt 1,212–1,444) were used for probe templates. An antidigoxigenin antibody linked to alkaline phosphatase (Dako) and NBT/BCIP (nitro blue tetrazolium chloride/5-bromo-4-chloro-3-indolyl phosphate; Dako) substrate was used to detect hybridization signals. All sections were developed for 1 h. Images were taken with a dissection microscope (SZ61; Olympus) equipped with a digital camera (DP20; Olympus) and with an upright microscope (BX51; Olympus) equipped with a UPlan SApo 20× NA 0.75 objective lens and a CCD camera (DP72; Olympus).

Quantitative Western blotting

Bands on blotted membranes were visualized with a cooled CCD camera (Light-Capture II; ATTO), and the optimal specific bands were analyzed with the CS Analyzer 3.0 software (ATTO). For calibration, immunopurified PSD-95–GFP and PSD-93–β-GFP from transfected HEK293 cells were quantitated by Coomassie brilliant staining using BSA.

Subcellular fractionation

The method was basically followed as described previously (Carlin et al., 1980). In brief, five rat adult brains were homogenized in buffer containing 320 mM sucrose and 10 mM Hepes-NaOH, pH 7.4 (containing 0.2 mM PMSF). Homogenate was centrifuged for 10 min at 1,000 *g* to remove crude nuclear fraction (P1). The supernatant (S1) was centrifuged at 9,000 *g* for 15 min to produce a pellet (P2) and supernatant (S2). The S2 was centrifuged at 100,000 *g* for 1 h to produce a pellet (P3; microsomal fraction) and supernatant (S3). The P2 fraction was resuspended in the homogenization buffer. Discontinuous sucrose gradients containing 3 ml of the resuspended P2 material and 3 ml each of 0.8, 1.0, and 1.2 M sucrose solutions in 10 mM Hepes-NaOH, pH 7.4, were run for 2 h at 58,000 *g* (SW41 rotor; Beckman Coulter). The band between 1.0 and 1.2 M sucrose was obtained as a synaptosome fraction. This synaptosome fraction was extracted with ice-cold 0.5% Triton X-100 in 0.16 M sucrose and 6 mM Tris-HCl, pH 8.1, and then centrifuged at 32,800 *g* for 20 min to divide into soluble and insoluble fractions (Ins1; PSD-1). The pellet was resuspended in 0.5% Triton X-100, 0.16 M sucrose, and 6 mM Tris-HCl, pH 8.1, and centrifuged at 200,000 *g* for 1 h to produce a pellet (Ins2; PSD-2). 50 µg of proteins of each fraction was analyzed by Western blotting.

Statistical analysis

The results are expressed as mean ± SD. Statistical comparisons between groups were performed by the Student's *t* test.

Online supplemental material

Fig. S1 shows that synaptic PSD-95 accumulation upon activity blockade does not require protein synthesis. Fig. S2 shows the specific detection of PSD-95 palmitoylation by biochemical approaches. Fig. S3 shows that DHHC2 and -3 and PSD-95 dominantly express as compared with other family proteins in the hippocampus. Fig. S4 shows that DHHC2 translocates near the postsynaptic sites upon activity blockade. Fig. S5 shows that DHHC2 and PSD-95 are necessary for homeostatic increase of GluR2 as well as GluR1. Video 1 shows PSD-95–GFP dynamics in neurons by time-lapse TIRFM imaging and shows the increased accumulation of PSD-95–GFP upon Kyn treatment. Video 2 shows that CHX treatment does not inhibit Kyn-induced PSD-95–GFP increase at the synapse. Video 3 shows that activity-sensitive trafficking of PSD-95 is regulated by DHHC2. Video 4 shows activity-sensitive trafficking of DHHC2. Video 5 shows the specificity of pH-GluR1 imaging. Video 6 shows AMPAR (pH-GluR1) dynamics by time-lapse TIRFM imaging. Video 7 shows that pH-GluR1 intensity gradually and continually increases over 12 h upon TTX treatment. Video 8 shows the

Downloaded from jcb.rupress.org on April 25, 2010

Published July 13, 2009

requirement of palmitoylating activity of DHHC2 for homeostatic increase of GluR1. Video 9 shows the requirement of PSD-95 palmitoylation for the homeostatic increase of GluR1. Online supplemental material is available at http://www.jcb.org/cgi/content/full/jcb.200903101/DC1.

We thank K. Imoto (National Institute for Physiological Sciences, Okazaki, Aichi, Japan) and M. Nishijima (National Institute of Health Sciences, Setagaya-ku,Tokyo, Japan and Japan Science and Technology Agency, Chiyoda-ku, Tokyo, Japan) for suggestions and encouragement, K. Kaibuchi for sharing reagents, F. Perez (Institut Curie, Paris, France), A.S. Kato (Eli Lilly and Company, Indianapolis, IN), and T. Watanabe (Nagoya University, Chikusa-ku, Nagoya, Japan) for valuable suggestions, and N. Takahashi for technical support.

J. Noritake and R. Tsutsumi are supported by the Japan Society for the Promotion of Science. Y. Fukata is supported by grants from the Human Frontier Science Program (HFSP; CDA0015-07) and Ministry of Education, Culture, Sports, Science and Technology (MEXT; 21680029). M. Fukata is also supported by grants from the HFSP (RGY0059-06) and MEXT (20670005, 20022043, and 20054022).

Submitted: 18 March 2009
Accepted: 11 June 2009

References

Ashby, M.C., S.A. De La Rue, G.S. Ralph, J. Uney, G.L. Collingridge, and J.M. Henley. 2004. Removal of AMPA receptors (AMPARs) from synapses is preceded by transient endocytosis of extrasynaptic AMPARs. *J. Neurosci.* 24:5172–5176.

Bartels, D.J., D.A. Mitchell, X. Dong, and R.J. Deschenes. 1999. Erf2, a novel gene product that affects the localization and palmitoylation of Ras2 in *Saccharomyces cerevisiae*. *Mol. Cell. Biol.* 19:6775–6787.

Carlin, R.K., D.J. Grab, R.S. Cohen, and P. Siekevitz. 1980. Isolation and characterization of postsynaptic densities from various brain regions: enrichment of different types of postsynaptic densities. *J. Cell Biol.* 86:831–845.

Chen, L., D.M. Chetkovich, R.S. Petralia, N.T. Sweeney, Y. Kawasaki, R.J. Wenthold, D.S. Bredt, and R.A. Nicoll. 2000. Stargazin regulates synaptic targeting of AMPA receptors by two distinct mechanisms. *Nature.* 408:936–943.

Chisari, M., D.K. Saini, V. Kalyanaraman, and N. Gautam. 2007. Shuttling of G protein subunits between the plasma membrane and intracellular membranes. *J. Biol. Chem.* 282:24092–24098.

El-Husseini, Ael-D., and D.S. Bredt. 2002. Protein palmitoylation: a regulator of neuronal development and function. *Nat. Rev. Neurosci.* 3:791–802.

El-Husseini, A.E., E. Schnell, D.M. Chetkovich, R.A. Nicoll, and D.S. Bredt. 2000. PSD-95 involvement in maturation of excitatory synapses. *Science.* 290:1364–1368.

El-Husseini, Ael-D., E. Schnell, S. Dakoji, N. Sweeney, Q. Zhou, O. Prange, C. Gauthier-Campbell, A. Aguilera-Moreno, R.A. Nicoll, and D.S. Bredt. 2002. Synaptic strength regulated by palmitate cycling on PSD-95. *Cell.* 108:849–863.

Elias, G.M., L. Funke, V. Stein, S.G. Grant, D.S. Bredt, and R.A. Nicoll. 2006. Synapse-specific and developmentally regulated targeting of AMPA receptors by a family of MAGUK scaffolding proteins. *Neuron.* 52:307–320.

Fang, C., L. Deng, C.A. Keller, M. Fukata, Y. Fukata, G. Chen, and B. Luscher. 2006. GODZ-mediated palmitoylation of GABA(A) receptors is required for normal assembly and function of GABAergic inhibitory synapses. *J. Neurosci.* 26:12758–12768.

Fernandez-Hernando, C., M. Fukata, P.N. Bernatchez, Y. Fukata, M.I. Lin, D.S. Bredt, and W.C. Sessa. 2006. Identification of Golgi-localized acyl transferases that palmitoylate and regulate endothelial nitric oxide synthase. *J. Cell Biol.* 174:369–377.

Firestein, B.L., S.E. Craven, and D.S. Bredt. 2000. Postsynaptic targeting of MAGUKs mediated by distinct N-terminal domains. *Neuroreport.* 11:3479–3484.

Fukata, M., Y. Fukata, H. Adesnik, R.A. Nicoll, and D.S. Bredt. 2004. Identification of PSD-95 palmitoylating enzymes. *Neuron.* 44:987–996.

Fukata, Y., A.V. Tzingounis, J.C. Trinidad, M. Fukata, A.L. Burlingame, R.A. Nicoll, and D.S. Bredt. 2005. Molecular constituents of neuronal AMPA receptors. *J. Cell Biol.* 169:399–404.

Fukata, Y., T. Iwanaga, and M. Fukata. 2006. Systematic screening for palmitoyl transferase activity of the DHHC protein family in mammalian cells. *Methods.* 40:177–182.

Funke, L., S. Dakoji, and D.S. Bredt. 2005. Membrane-associated guanylate kinases regulate adhesion and plasticity at cell junctions. *Annu. Rev. Biochem.* 74:219–245.

Hayashi, T., G. Rumbaugh, and R.L. Huganir. 2005. Differential regulation of AMPA receptor subunit trafficking by palmitoylation of two distinct sites. *Neuron.* 47:709–723.

Hemsley, P.A., and C.S. Grierson. 2008. Multiple roles for protein palmitoylation in plants. *Trends Plant Sci.* 13:295–302.

Hemsley, P.A., A.C. Kemp, and C.S. Grierson. 2005. The TIP GROWTH DEFECTIVE1 S-acyl transferase regulates plant cell growth in *Arabidopsis*. *Plant Cell.* 17:2554–2563.

Hughes, T.E., H. Zhang, D.E. Logothetis, and C.H. Berlot. 2001. Visualization of a functional Galpha q-green fluorescent protein fusion in living cells. Association with the plasma membrane is disrupted by mutational activation and by elimination of palmitoylation sites, but not be activation mediated by receptors or AlF4. *J. Biol. Chem.* 276:4227–4235.

Kang, R., J. Wan, P. Arstikaitis, H. Takahashi, K. Huang, A.O. Bailey, J.X. Thompson, A.F. Roth, R.C. Drisdel, R. Mastro, et al. 2008. Neural palmitoyl-proteomics reveals dynamic synaptic palmitoylation. *Nature.* 456:904–909.

Keller, C.A., X. Yuan, P. Panzanelli, M.L. Martin, M. Alldred, M. Sassoe-Pognetto, and B. Luscher. 2004. The gamma2 subunit of GABA(A) receptors is a substrate for palmitoylation by GODZ. *J. Neurosci.* 24:5881–5891.

Kennedy, M.B. 2000. Signal-processing machines at the postsynaptic density. *Science.* 290:750–754.

Kim, E., and M. Sheng. 2004. PDZ domain proteins of synapses. *Nat. Rev. Neurosci.* 5:771–781.

Linder, M.E., and R.J. Deschenes. 2004. Model organisms lead the way to protein palmitoyltransferases. *J. Cell Sci.* 117:521–526.

Linder, M.E., and R.J. Deschenes. 2007. Palmitoylation: policing protein stability and traffic. *Nat. Rev. Mol. Cell Biol.* 8:74–84.

Lobo, S., W.K. Greentree, M.E. Linder, and R.J. Deschenes. 2002. Identification of a Ras palmitoyltransferase in *Saccharomyces cerevisiae*. *J. Biol. Chem.* 277:41268–41273.

Luo, J.H., Z.Y. Fu, G. Losi, B.G. Kim, K. Prybylowski, B. Vissel, and S. Vicini. 2002. Functional expression of distinct NMDA channel subunits tagged with green fluorescent protein in hippocampal neurons in culture. *Neuropharmacology.* 42:306–318.

Luthi, A., H. Van der Putten, F.M. Botteri, I.M. Mansuy, M. Meins, U. Frey, G. Sansig, C. Portet, M. Schmutz, M. Schroder, et al. 1997. Endogenous serine protease inhibitor modulates epileptic activity and hippocampal long-term potentiation. *J. Neurosci.* 17:4688–4699.

Mansilla, F., K. Birkenkamp-Demtroder, M. Kruhoffer, F.B. Sorensen, C.L. Andersen, P. Laiho, L.A. Aaltonen, H.W. Verspaget, and T.F. Orntoft. 2007. Differential expression of DHHC9 in microsatellite stable and instable human colorectal cancer subgroups. *Br. J. Cancer.* 96:1896–1903.

Mansouri, M.R., L. Marklund, P. Gustavsson, E. Davey, B. Carlsson, C. Larsson, I. White, K.H. Gustavson, and N. Dahl. 2005. Loss of ZDHHC15 expression in a woman with a balanced translocation t(X;15)(q13.3;cen) and severe mental retardation. *Eur. J. Hum. Genet.* 13:970–977.

Masuda, K., H. Itoh, T. Sakihama, C. Akiyama, K. Takahashi, R. Fukuda, T. Yokomizo, T. Shimizu, T. Kodama, and T. Hamakubo. 2003. A combinatorial G protein-coupled receptor reconstitution system on budded baculovirus. Evidence for Galpha and Galphao coupling to a human leukotriene B4 receptor. *J. Biol. Chem.* 278:24552–24562.

Miesenbock, G., D.A. De Angelis, and J.E. Rothman. 1998. Visualizing secretion and synaptic transmission with pH-sensitive green fluorescent proteins. *Nature.* 394:192–195.

Migaud, M., P. Charlesworth, M. Dempster, L.C. Webster, A.M. Watabe, M. Makhinson, Y. He, M.F. Ramsay, R.G. Morris, J.H. Morrison, et al. 1998. Enhanced long-term potentiation and impaired learning in mice with mutant postsynaptic density-95 protein. *Nature.* 396:433–439.

Mukai, J., H. Liu, R.A. Burt, D.E. Swor, W.S. Lai, M. Karayiorgou, and J.A. Gogos. 2004. Evidence that the gene encoding ZDHHC8 contributes to the risk of schizophrenia. *Nat. Genet.* 36:725–731.

Mukai, J., A. Dhilla, L.J. Drew, K.L. Stark, L. Cao, A.B. MacDermott, M. Karayiorgou, and J.A. Gogos. 2008. Palmitoylation-dependent neurodevelopmental deficits in a mouse model of 22q11 microdeletion. *Nat. Neurosci.* 11:1302–1310.

Nakagawa, M., M. Fukata, M. Yamaga, N. Itoh, and K. Kaibuchi. 2001. Recruitment and activation of Rac1 by the formation of E-cadherin-mediated cell-cell adhesion sites. *J. Cell Sci.* 114:1829–1838.

Nicoll, R.A., S. Tomita, and D.S. Bredt. 2006. Auxiliary subunits assist AMPA-type glutamate receptors. *Science.* 311:1253–1256.

O'Brien, R.J., S. Kamboj, M.D. Ehlers, K.R. Rosen, G.D. Fischbach, and R.L. Huganir. 1998. Activity-dependent modulation of synaptic AMPA receptor accumulation. *Neuron.* 21:1067–1078.

Ohyama, T., P. Verstreken, C.V. Ly, T. Rosenmund, A. Rajan, A.C. Tien, C. Haueter, K.L. Schulze, and H.J. Bellen. 2007. Huntingtin-interacting

Downloaded from jcb.rupress.org on April 25, 2010

Published July 13, 2009

protein 14, a palmitoyl transferase required for exocytosis and targeting of CSP to synaptic vesicles. *J. Cell Biol.* 179:1481–1496.

Oyama, T., Y. Miyoshi, K. Koyama, H. Nakagawa, T. Yamori, T. Ito, H. Matsuda, H. Arakawa, and Y. Nakamura. 2000. Isolation of a novel gene on 8p21.3-22 whose expression is reduced significantly in human colorectal cancers with liver metastasis. *Genes Chromosomes Cancer.* 29:9–15.

Parker, M.J., S. Zhao, D.S. Bredt, J.R. Sanes, and G. Feng. 2004. PSD93 regulates synaptic stability at neuronal cholinergic synapses. *J. Neurosci.* 24:378–388.

Ponimaskin, E., G. Dityateva, M.O. Ruonala, M. Fukata, Y. Fukata, F. Kobe, F.S. Wouters, M. Delling, D.S. Bredt, M. Schachner, and A. Dityatev. 2008. Fibroblast growth factor-regulated palmitoylation of the neural cell adhesion molecule determines neuronal morphogenesis. *J. Neurosci.* 28:8897–8907.

Raymond, F.L., P.S. Tarpey, S. Edkins, C. Tofts, S. O'Meara, J. Teague, A. Butler, C. Stevens, S. Barthorpe, G. Buck, et al. 2007. Mutations in ZDHHC9, which encodes a palmitoyltransferase of NRAS and HRAS, cause X-linked mental retardation associated with a Marfanoid habitus. *Am. J. Hum. Genet.* 80:982–987.

Resh, M.D. 2006. Palmitoylation of ligands, receptors, and intracellular signaling molecules. *Sci. STKE.* doi:10.1126/stke.3592006re14.

Rocks, O., A. Peyker, M. Kahms, P.J. Verveer, C. Koerner, M. Lumbierres, J. Kuhlmann, H. Waldmann, A. Wittinghofer, and P.I. Bastiaens. 2005. An acylation cycle regulates localization and activity of palmitoylated Ras isoforms. *Science.* 307:1746–1752.

Rocks, O., A. Peyker, and P.I. Bastiaens. 2006. Spatio-temporal segregation of Ras signals: one ship, three anchors, many harbors. *Curr. Opin. Cell Biol.* 18:351–357.

Roth, A.F., Y. Feng, L. Chen, and N.G. Davis. 2002. The yeast DHHC cysteine-rich domain protein Akr1p is a palmitoyl transferase. *J. Cell Biol.* 159:23–28.

Roth, A.F., J. Wan, A.O. Bailey, B. Sun, J.A. Kuchar, W.N. Green, B.S. Phinney, J.R. Yates III, and N.G. Davis. 2006. Global analysis of protein palmitoylation in yeast. *Cell.* 125:1003–1013.

Saitoh, R., T. Ohtomo, Y. Yamada, N. Kamada, J. Nezu, N. Kimura, S. Funahashi, K. Furugaki, T. Yoshino, Y. Kawase, et al. 2007. Viral envelope protein gp64 transgenic mouse facilitates the generation of monoclonal antibodies against exogenous membrane proteins displayed on baculovirus. *J. Immunol. Methods.* 322:104–117.

Shaner, N.C., P.A. Steinbach, and R.Y. Tsien. 2005. A guide to choosing fluorescent proteins. *Nat. Methods.* 2:905–909.

Stellwagen, D., and R.C. Malenka. 2006. Synaptic scaling mediated by glial TNF-alpha. *Nature.* 440:1054–1059.

Stowers, R.S., and E.Y. Isacoff. 2007. *Drosophila* huntingtin-interacting protein 14 is a presynaptic protein required for photoreceptor synaptic transmission and expression of the palmitoylated proteins synaptosome-associated protein 25 and cysteine string protein. *J. Neurosci.* 27:12874–12883.

Tomita, S., M. Fukata, R.A. Nicoll, and D.S. Bredt. 2004. Dynamic interaction of stargazin-like TARPs with cycling AMPA receptors at synapses. *Science.* 303:1508–1511.

Topinka, J.R., and D.S. Bredt. 1998. N-terminal palmitoylation of PSD-95 regulates association with cell membranes and interaction with K+ channel, Kv1.4. *Neuron.* 20:125–134.

Tsutsumi, R., Y. Fukata, J. Noritake, T. Iwanaga, F. Perez, and M. Fukata. 2009. Identification of G protein alpha subunit-palmitoylating enzyme. *Mol. Cell. Biol.* 29:435–447.

Turrigiano, G.G., K.R. Leslie, N.S. Desai, L.C. Rutherford, and S.B. Nelson. 1998. Activity-dependent scaling of quantal amplitude in neocortical neurons. *Nature.* 391:892–896.

Wedegaertner, P.B., and H.R. Bourne. 1994. Activation and depalmitoylation of Gs alpha. *Cell.* 77:1063–1070.

Wessel, D., and U.I. Flugge. 1984. A method for the quantitative recovery of protein in dilute solution in the presence of detergents and lipids. *Anal. Biochem.* 138:141–143.

Yamamoto, Y., Y. Chochi, H. Matsuyama, S. Eguchi, S. Kawauchi, T. Furuya, A. Oga, J.J. Kang, K. Naito, and K. Sasaki. 2007. Gain of 5p15.33 is associated with progression of bladder cancer. *Oncology.* 72:132–138.

Yanai, A., K. Huang, R. Kang, R.R. Singaraja, P. Arstikaitis, L. Gan, P.C. Orban, A. Mullard, C.M. Cowan, L.A. Raymond, et al. 2006. Palmitoylation of huntingtin by HIP14 is essential for its trafficking and function. *Nat. Neurosci.* 9:824–831.

Yudowski, G.A., M.A. Puthenveedu, D. Leonoudakis, S. Panicker, K.S. Thorn, E.C. Beattie, and M. von Zastrow. 2007. Real-time imaging of discrete exocytic events mediating surface delivery of AMPA receptors. *J. Neurosci.* 27:11112–11121.

Downloaded from jcb.rupress.org on April 25, 2010

Research article

Adoptive immunotherapy with liver allograft–derived lymphocytes induces anti-HCV activity after liver transplantation in humans and humanized mice

Masahiro Ohira,[1,2] Kohei Ishiyama,[1,2] Yuka Tanaka,[1,2] Marlen Doskali,[1,2] Yuka Igarashi,[1,2] Hirotaka Tashiro,[1,2] Nobuhiko Hiraga,[2,3] Michio Imamura,[2,3] Naoya Sakamoto,[4] Toshimasa Asahara,[1,2] Kazuaki Chayama,[2,3] and Hideki Ohdan[1,2]

[1]Department of Surgery, Division of Frontier Medical Science, Programs for Biomedical Research, Graduate School of Biomedical Sciences, [2]Liver Research Project Center, and [3]Department of Medicine and Molecular Science, Division of Frontier Medical Science, Programs for Biomedical Research, Graduate School of Biomedical Sciences, Hiroshima University, Minami-ku, Hiroshima, Japan. [4]Department of Gastroenterology and Hepatology, Tokyo Medical and Dental University, Bunkyo-ku, Tokyo, Japan.

After liver transplantation in HCV-infected patients, the virus load inevitably exceeds pre-transplantation levels. This phenomenon reflects suppression of the host-effector immune responses that control HCV replication by the immunosuppressive drugs used to prevent rejection of the transplanted liver. Here, we describe an adoptive immunotherapy approach, using lymphocytes extracted from liver allograft perfusate (termed herein liver allograft–derived lymphocytes), which includes an abundance of NK/NKT cells that mounted an anti-HCV response in HCV-infected liver transplantation recipients, despite the immunosuppressive environment. This therapy involved intravenously injecting patients 3 days after liver transplantation with liver allograft–derived lymphocytes treated with IL-2 and the CD3-specific mAb OKT3. During the first month after liver transplantation, the HCV RNA titers in the sera of recipients who received immunotherapy were markedly lower than those in the sera of recipients who did not receive immunotherapy. We further explored these observations in human hepatocyte–chimeric mice, in which mouse hepatocytes were replaced by human hepatocytes. These mice unfailingly developed HCV infections after inoculation with HCV-infected human serum. However, injection of human liver–derived lymphocytes treated with IL-2/OKT3 completely prevented HCV infection. Furthermore, an in vitro study using genomic HCV replicon–containing hepatic cells revealed that IFN-γ–secreting cells played a pivotal role in such anti-HCV responses. Thus, our study presents what we believe to be a novel paradigm for the inhibition of HCV replication in HCV-infected liver transplantation recipients.

Introduction

Liver failure and hepatocellular carcinoma (HCC) due to chronic hepatitis C infection are the most common indications for liver transplantation (LT), and the incidences of both have been projected to increase further in the future. Recurrent HCV infection of the allograft is universal, occurs immediately after LT, and is associated with accelerated progression to cirrhosis, graft loss, and death (1, 2). This reflects the suppression of those host-effector immune responses that usually control HCV replication, suggesting that the immunosuppressive environment may play a major role in the rapid progression of recurrent HCV infection after LT (3, 4). Further, the immunosuppressive condition described above is considered to increase the incidence of cancer recurrence after LT in HCC patients. We recently proposed the novel strategy of adjuvant immunotherapy for preventing the recurrence of HCC after LT; this immunotherapy involves intravenously injecting LT recipients with activated liver allograft–derived NK cells (5, 6). Since the immunosuppressive regimen currently used after LT reduces the adaptive immune components but effectively maintains the innate components of cellular immunity (7–9), the augmentation of the NK cell response, which is thought to play a pivotal role in innate immunity, may be a promising immunotherapeutic approach (6). We confirmed that the IL-2/anti-CD3 mAb–treated (IL-2/OKT3–treated) liver allograft–derived NK cells expressed a significantly high level of the tumor necrosis factor–related apoptosis-inducing ligand (TRAIL), which is a critical molecule for tumor cell killing. Further, these cells showed high cytotoxicity against HCC cells, with no such effect on normal cells (5). After obtaining approval from the ethical committee of our institute, we successfully administered adoptive immunotherapy with IL-2/OKT3–treated liver lymphocytes to liver cirrhosis patients with HCC in a phase I trial. Although the long-term benefits of this approach with regard to the control of HCC recurrence after LT remain to be elucidated, this trial provided a unique opportunity to study whether the adoptive administration of IL-2/OKT3–treated liver lymphocytes could also mount an anti-HCV response in HCV-infected LT recipients.

Previous studies have highlighted the important roles of innate lymphocytes in developing immunity against hepatotropic viruses, including HCV (10, 11). In this regard, it is known that patients with chronic HCV infection show diminished NK and NKT cell responses (12–14). In the case of an LT, it has recently been reported that the host CD56$^+$ innate lymphocyte population,

Conflict of interest: The authors have declared that no conflict of interest exists.
Citation for this article: *J. Clin. Invest.* **119**:3226–3235 (2009). doi:10.1172/JCI38374.

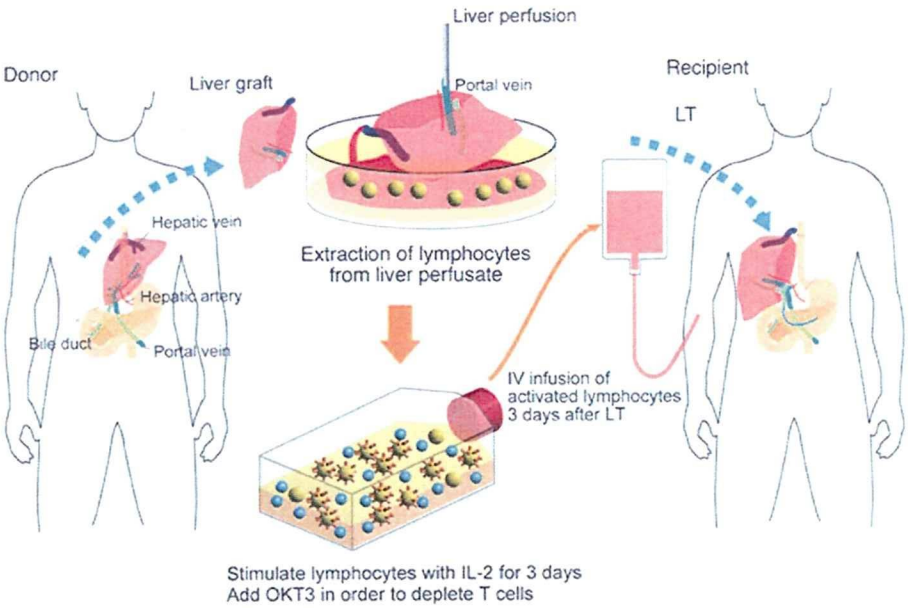

Figure 1
Schematic outline of adoptive immunotherapy with lymphocytes extracted from liver allograft perfusate. The therapy involved giving an intravenous injection of IL-2/OKT3–treated liver lymphocytes to LT recipients. The lymphocytes were extracted from the donor liver graft perfusate. After 3 days of culture with IL-2 (100 JRU/ml), the activated liver NK cell–enriched lymphocytes were administered to the LT recipients through venous circulation. OKT3 (1 μg/ml) was added to the culture medium 1 day before this administration in order to prevent GVHD.

consisting of NK and NKT cells, is appreciably associated with the severity of HCV recurrence after LT (15). These insights into the immunopathogenesis of HCV recurrence indicate that the innate immune components mentioned above are potential targets for therapeutic manipulation. In this study, we have demonstrated for the first time to our knowledge that adoptive immunotherapy with IL-2/OKT3–treated liver lymphocytes, including abundant NK and NKT cells, shows anti-HCV activity after LT, even in an immunosuppressive environment.

Results

Adoptive transfer of IL-2/OKT3–treated liver lymphocytes. The human liver contains a significant number of resident lymphocytes. These cells include abundant $CD56^+$ NK and NKT cells, many of which differ phenotypically and functionally from the circulating cells (14, 16). In our previous study, we performed ex vivo perfusion of the liver through the portal vein, which was necessary in order to flush blood from the liver graft before implantation. Liver-resident lymphocytes were then extracted from the perfusates (number of lymphocytes extracted from normal liver perfusates, 0.5 ± 0.1 cells per gram of liver weight; $n = 14$) (5). Proportions of $CD56^+CD3^-$ NK cells and $CD56^+CD3^+$ NKT cells among the lymphocytes extracted from the liver perfusates (NK cells, 46.4% ± 4.2%; NKT cells, 17.2% ± 2.3%; $n = 14$) were significantly ($P < 0.05$) higher than those among the lymphocytes derived from the peripheral blood of the same donors (NK cells, 21.9% ± 3.7%; NKT cells, 3.8% ± 0.9%; $n = 14$). Extensive preclinical studies have shown that liver allograft–derived resident NK cells mediate remarkably higher cytotoxic activity against HCC cells than do peripheral blood NK cells (5). On this basis, we undertook a clinical trial of adjuvant immunotherapy with IL-2/OKT3–treated liver lymphocytes for preventing the recurrence of HCC after LT in 14 recipients with HCC (Figure 1 and Tables 1 and 2). The therapy involved administering a single intravenous injection of IL-2/OKT3–treated liver lymphocytes to recipients 3 days after LT ($2–5 \times 10^8$ cells injected per subject). In order to prevent graft-versus-host disease (GVHD), i.e., to inactivate $CD3^+$ alloreactive T cells, we added an anti-CD3 mAb, OKT3, to the culture medium a day before the inoculation. During the follow-up period (mean, 23.4 months; range, 10.7–32.9 months), neither any remarkable adverse effects nor rejection episodes occurred. All 14 subjects who received the immunotherapy were alive without recurrence of HCC after LT (including 5 patients with HCC exceeding the Milan criteria; ref. 17). At our institute, the survival rate and recurrence rate of historical control patients with HCC exceeding the Milan criteria were 78% (30 of 37) and 10.8% (4 of 37), respectively. The lymphocytes in the peripheral blood of LT recipients who received immunotherapy in the early postoperative period showed significantly enhanced cytotoxicity against an HCC cell line (HepG2) as compared with those in the peripheral blood of LT recipients who did not receive the therapy in the same period (Figure 2A). Although the gross proportions of NK/NKT cells in the peripheral blood of patients treated with immunotherapy did not differ from those in the peripheral blood of untreated patients, the proportions of $TRAIL^+$ NK cells significantly increased after immunotherapy in the peripheral blood of the former patients. This increase in the $TRAIL^+$ NK cells in the peripheral blood lymphocytes was not observed in untreated patients (Figure 2B). Furthermore, there was a significant correlation between the frequency of $TRAIL^+$ NK cells in the peripheral blood lymphocytes and the NK cytolytic activity of the peripheral blood lymphocytes at 7 days after LT (Spearman rank-order correlation coefficient = 0.54, $P = 0.01$; Figure 2C), indicating the anti-HCC effect of adoptively injected $TRAIL^+$ NK cells. It would be pertinent to conduct additional clinical trials of this immunotherapy for preventing HCC recurrence after LT.

Anti-HCV activity after adoptive immunotherapy. Of the 14 LT recipients who received the immunotherapy, 7 had chronic HCV infection. During the period of this trial, 5 other HCV-infected LT recipients who did not agree to receive immunotherapy served as controls; the background of the controls, including HCV genotype, age, and immunosuppressive therapy, was similar to that of the immunotherapy recipients (Table 3). It has been reported

Table 1
Recipient and tumor characteristics

Patient no.	Age (yr)	Sex	MELD	Hepatitis virus infection	HLA A	HLA B	HLA C	Milan criteria	AFP (ng/ml)	PIVKA-II (AU/ml)	Tumor no.	Maximum tumor size (mm)	Path. vascular invasion	Path. stage	Postop. months	Outcome
1	67	M	19	B	24,-	13,40	03,-	OUT	–	2,584	5	35	–	III	32.9	Alive
2	53	M	16	B	2603,3303	4002,4403	0304,1403	IN	25.3	43	4	11	–	II	31.0	Alive
3	54	M	7	B	0206,3101	3501,5101	0303,1402	OUT	5.7	213	11	26	–	III	29.4	Alive
4	64	F	16	C	2601,2603	3501,4801	0303,-	IN	5.9	142	–	–	–	–	28.5	Alive
5	59	F	14	B	0206,2601	4002,5502	0102,0304	OUT	<5	65	1	13	b1	II	27.8	Alive
6	47	F	8	C	2402,2601	3501,5201	0303,1202	IN	18	46	3	12	–	II	26.2	Alive
7	57	M	29	B	2402,3101	5101,5201	1202,1402	IN	40.3	514	1	25	–	II	25.4	Alive
8	65	F	18	C	1101,2402	5401,5901	0102,-	IN	–	–	3	6	–	II	24.4	Alive
9	60	F	8	–	1101,3001	1302,4006	0602,0801	OUT	32.8	3,026	2	40	vv1	IVA	22.7	Alive
10	56	M	8	C	2402,3303	5201,5801	0302,1202	OUT	–	304	11	22	–	III	19.1	Alive
11	56	M	9	C	0207,-	4601,-	0102,-	IN	47	20	3	25	–	III	17.5	Alive
12	58	M	22	C	1101,3101	1501,3501	0102,0415	IN	–	62	1	17	–	I	16.5	Alive
13	59	M	6	C	1101,2402	1507,1501	0303,0401	IN	202.9	19	3	16	–	II	15.8	Alive
14	51	M	16	B	1101,2601	4002,5401	0102,0304	IN	–	29	–	–	–	–	10.7	Alive

The Milan criteria specifies that liver cancer patients with a single tumor of 5 or fewer centimeters in diameter or 3 or fewer tumors, each no more than 3 cm in diameter, and with no macrovascular invasion, can expect an excellent outcome after LT, with only a 10% risk of cancer recurrence (31). AFP, alpha fetoprotein; F, female; M, male; MELD, model for end-stage liver disease; PIVKA-II, protein induced by vitamin K absence; Path., pathological; Postop., postoperative.

that HCV RNA concentrations sharply decrease a day after LT and increase rapidly thereafter (3). In some of the patients, who did not receive the immunotherapy, HCV RNA titers remained lower than that of the pretransplant titer 1 week after LT, suggesting the individual variation of increasing tempo. However, in almost all patients, HCV RNA titers exceeded the pretransplantation levels by 2 weeks after LT. Notably, HCV infection disappeared in 2 LT recipients after the immunotherapy, but this was not observed in the case of any HCV-infected LT recipients who did not receive the therapy. In one of these patients (who had the lowest HCV RNA levels before LT), HCV RNA has not been detected to date (20 months after LT), even with a qualitative assay. In the other patient, HCV RNA became detectable at 2 months after LT. On the other hand, the 2 patients with the highest HCV viral loads did not respond at all to the immunotherapy. Thus, the effects of immunotherapy were dependent on the HCV virus load before LT, probably because of the proportion of effectors and targets. All patients with HCV viremia are currently being treated with pegylated IFN-α2b and ribavirin. Nevertheless, during the first month after LT, the HCV RNA titers in the sera of LT recipients who received the immunotherapy were statistically lower than those in the sera of LT recipients who did not receive the therapy ($P < 0.05$) (Figure 3). Among the LT recipients who received the immunotherapy, at 2 weeks after LT, HCV RNA remained undetectable in 4 patients (responders), whereas it was detectable in the other 3 patients (nonresponders). The serum ALT levels did not differ between the responders and nonresponders (Supplemental Figure 1; supplemental material available online with this article; doi:10.1172/JCI38374DS1), suggesting that the immunotherapy did not inhibit HCV RNA by injuring HCV-infected hepatocytes.

In vitro evidence to prove the anti-HCV activity of IL-2/OKT3–treated liver lymphocytes by using HCV replicon–containing hepatic cells. The liver allograft–derived lymphocytes were cultured in complete medium with and without IL-2 for 3 days. This was followed by adding OKT3 to the culture medium 1 day before coculturing the lymphocytes with HCV replicon–containing hepatic cells in a transwell system, at an indicated time. While the freshly isolated liver allograft–derived lymphocytes inhibited HCV replication in the HCV replicon–containing hepatic cells to some extent, the cultivation of these lymphocytes with IL-2/OKT3 markedly promoted anti-HCV activity. Absence of exposure to either IL-2 or OKT3 resulted in reduced anti-HCV activity of the lymphocytes (OKT3 had a more profound influence than IL-2) (Figure 4A). When the lymphocytes were treated with IL-2 alone, the $CD56^+$ fraction, including NK and NKT cells, that had been isolated by magnetic cell sorting inhibited HCV replication more strongly than the $CD56^-$ fraction; further, the $CD3^-CD56^+$ NK cell and $CD3^+CD56^+$ NKT cell subfractions showed equivalent anti-HCV activity (Figure 4, B and C). On the other hand, when the lymphocytes were treated with both IL-2 and OKT3, the $CD56^+$ and $CD56^-$ fractions showed similar levels of anti-HCV activity (Figure 4B). After the treatment with IL-2 and OKT3, IFN-γ was the predominant cytokine in the culture supernatant of the lymphocytes (Figure 5A), and intracellular IFN-γ expression was induced in the $CD3^-CD56^+$ NK, $CD3^+CD56^+$ NKT, and $CD3^+CD56^-$ T cells (Figure 5B). There was no difference between the proportions of $TRAIL^+$ and $TRAIL^-$ $CD3^-CD56^+$ NK cells producing IFN-γ (Supplemental Figure 2). Adding mAb against IFN-γ to the coculture of lymphocytes with HCV replicon cells markedly weakened the anti-HCV effects. The incomplete restoration of the anti-HCV effect by anti–IFN-γ treat-

Table 2
Donor and graft characteristics

Donor no.	Donor age (yr)	Donor sex	HLA A	HLA B	HLA C	Relationship	Graft	Graft weight (g)	No. of cells administered (× 10^6)
1	41	M	24,-	07,40	03,07	Offspring	Right	608	172
2	24	M	2402,2603	4002,2603	0304,5201	Offspring	Right	658	38
3	51	F	0201,2402	0702,3901	0702,-	Spouse	Right	670	129
4	34	M	2601,2603	4001,4801	0303,0401	Offspring	Left	414	143
5	31	M	0206,2402	4002,5401	0102,0304	Offspring	Posterior	702	135
6	53	F	2402,-	5201,5401	0102,1202	Sibling	Right	538	411
7	24	M	2601,3101	4006,5201	0801,1202	Offspring	Right	642	350
8	34	M	1101,-	4001,5401	0102,1502	Offspring	Right	846	229
9	37	M	0201,1101	1501,4006	0702,0801	Offspring	Left	402	811
10	28	M	1101,3303	5502,5801	0102,0302	Offspring	Right	686	517
11	28	M	0207,2402	4601,5201	0102,5201	Offspring	Right	558	414
12	27	M	0201,1101	1501,3501	0303,0415	Offspring	Right	628	509
13	54	F	1101,2402	1501,1507	0303,0401	Sibling	Right	650	460
14	21	F	2601,2603	1501,5401	0102,0303	Offspring	Right	436	382

ment suggests the possibility that other inflammatory cytokines may also be responsible for the anti-HCV effect, although we have not defined them at present (Figure 5C). Thus, the vigorous anti-HCV activity of IL-2/OKT3–treated liver lymphocytes was dependent, at least in part, on their IFN-γ–secreting activity.

IFN-γ–secreting activity in LT recipients after adoptive immunotherapy. At 14 days after LT, the number of IFN-γ–secreting cells in the peripheral blood of LT recipients who received adoptive immunotherapy was significantly higher than that in the peripheral blood of LT recipients who did not receive immunotherapy during the trial period (Figure 6). This result was consistent with the results of the in vitro studies showing the crucial role of IFN-γ produced in IL-2/OKT3–treated liver lymphocytes.

In vivo evidence to prove the anti-HCV activity of adoptive immunotherapy by using HCV-infected human hepatocyte–chimeric mice. HCV-infected mice have previously been developed by inoculating HCV-infected human serum into chimeric urokinase-type plasminogen activator–SCID (uPA-SCID) mice with engrafted human hepatocytes (18). This HCV-infected mouse model has been reported to be useful for evaluating anti-HCV drugs such as IFN-α and anti-NS3 protease (19). We also generated a human hepatocyte-chimeric mouse model, in which mouse hepatocytes were almost completely replaced by human hepatocytes (20). These mice consistently developed long-term HCV infections, showing high viral titers after inoculation with HCV genotype 1b–infected human serum (50 μl/mouse) (Supplemental Figure 3). Intraperitoneal injection of IL-2/OKT3–treated liver lymphocytes (20 × 10^6 cells/mouse), at 2 weeks after inoculation with the infected serum, consistently prevented the development of HCV infection in the human hepatocyte-chimeric mice (Figure 7A). Such anti-HCV effects were countered by anti–IFN-γ neutralizing antibodies in some chimeric mice, suggesting the potential role played by IFN-γ in the anti-HCV effects of the immunotherapy. The administration of recombinant human IFN-γ markedly and consistently prevented the development of HCV infection in the human hepatocyte-chimeric mice. Once the HCV RNA became undetectable in the sera of chimeric mice receiving either IL-2/OKT3–treated liver lymphocytes or recombinant IFN-γ, it could not be detected again. The constant levels of human serum albumin in the chimeric mice indicated that neither the immunotherapy nor recombinant IFN-γ administration had significant adverse effects on human hepatocytes in those mice (Figure 7B). Once HCV infection had developed in the human hepatocyte-chimeric mice, who showed high titers of HCV RNA in their sera (over 10^3 copies/ml) 4 weeks after the inoculation of HCV-infected serum, the preventive effects of the adoptive immunotherapy or recombinant IFN-γ on HCV infection were no longer observed (Figure 7C).

Table 3
Characteristics of HCV-infected LT recipients that received and did not receive immunotherapy

No.	Age	Sex	HCV genotype	MELD	Pre–HCV RNA (KIU/ml)	Postoperative months	Immunosuppressant
With immunotherapy							
4	64	F	1b	16	210	29	Basiliximab+FK506+MMF
6	47	F	1b	8	5,000	26	Basiliximab+CsA+MMF
8	65	F	1b	18	2,400	24	Basiliximab+CsA+MMF
10	56	M	1b	8	970	19	Basiliximab+FK506+MMF
11	56	M	1b	9	1,700	17	Basiliximab+FK506+MMF
12	58	M	1b	22	19	17	Basiliximab+FK506+MMF
13	59	M	1b	6	2,200	16	Basiliximab+FK506+MMF
Without immunotherapy							
A	51	M	1b	27	420	42	Basiliximab+FK506+MMF
B	44	M	1b	10	1,600	32	Basiliximab+FK506+MMF
C	54	M	1b	8	180	22	Basiliximab+CsA+MMF
D	56	M	2a	10	470	20	Basiliximab+FK506+MMF
E	57	M	1b	12	3,200	6	Basiliximab+FK506+MMF

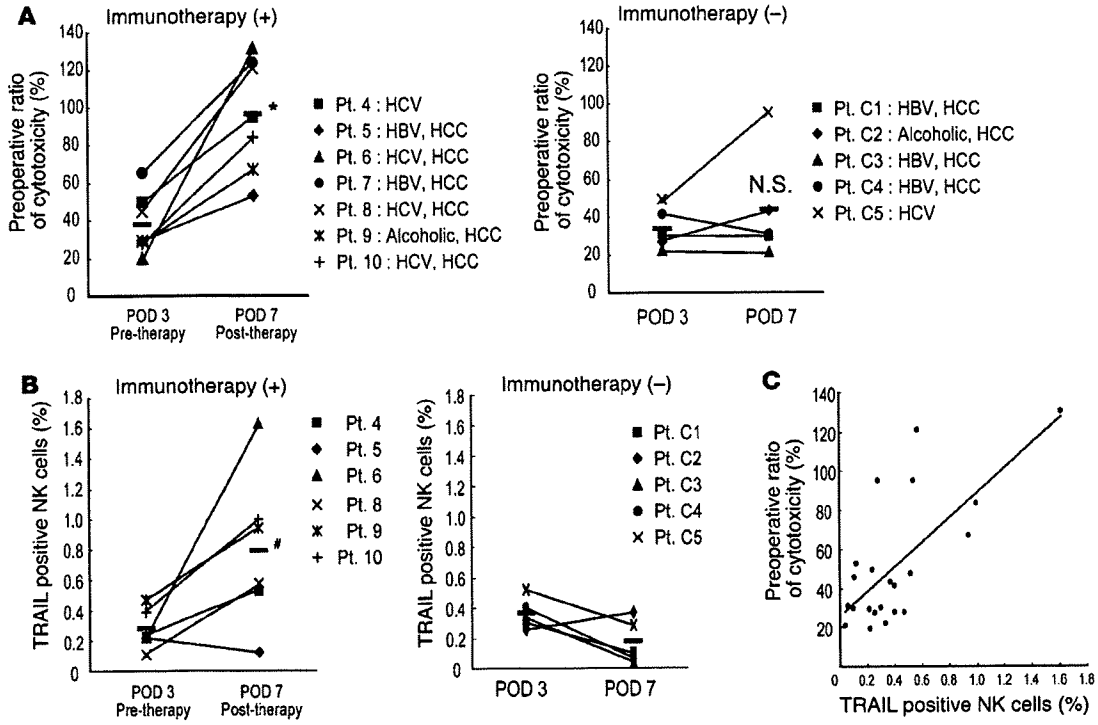

Figure 2

Adoptive immunotherapy with IL-2/OKT3–treated liver lymphocytes promoted the cytotoxic activity and TRAIL expression of NK cells in LT recipients. (**A**) The NK cytotoxic activities of the indicated effectors against their target cells were analyzed by the ^{51}Cr-release assay. The dot plot represents the NK cytotoxic activities of freshly isolated peripheral blood lymphocytes obtained from recipients who received immunotherapy (+) ($n = 7$) and did not receive immunotherapy (–) ($n = 5$) against HepG2 target cells (effector/target [E/T] ratio, 40:1) 3 and 7 days after LT. NK cytotoxic activities are represented as a proportion (percentage) of the preoperative cytotoxicity in each patient. Horizontal lines indicate the mean. Statistical analyses were performed using the 2-tailed, paired Student's *t* test. $^{*}P < 0.05$ for day 7 versus day 3. (**B**) The frequency of TRAIL^{+} NK cells increased remarkably in the peripheral blood of LT recipients who received the immunotherapy. Horizontal lines indicate the mean. Statistical analyses were performed using the Mann-Whitney *U* test. $^{\#}P = 0.013$ for immunotherapy group versus untreated group in postoperative day 7. (**C**) Correlation between TRAIL^{+} NK cell ratio and NK cytolytic activity after LT (Spearman rank-order correlation coefficient = 0.54, $P = 0.01$). Statistical analyses were performed using the Spearman rank-order correlation coefficient. The diagonal line indicates a linear regression line. Each dot indicates the cytotoxicity and TRAIL^{+} NK cell percentange of each patient. C1, control 1; POD, postoperative day; Pt., patient.

Discussion

The consequences of recurrent hepatitis C on the survival of graft and LT recipients can only be avoided by the development of safe and effective antiviral strategies that can not only prevent initial graft infection but also eradicate established hepatitis C recurrence (3, 4). With regard to initial graft infection, the circulating virions infect the liver graft immediately after LT. HCV RNA concentrations usually increase a few days after LT, reflecting active HCV replication in the liver graft. In general, in such an early phase of a viral infection, the first line of host defense may be effective in removing the virus; however, recent reports have indicated that HCV effectively escapes the innate immune system comprising NK and NKT cells, resulting in persistent infection (21, 22). It has been reported that cross-linking of CD81 on NK cells by the major envelope protein of HCV, HCV-E2, blocks NK cell activation, IFN-γ production, cytotoxic granule release, and proliferation (21). Engagement of CD81 on NK cells blocks tyrosine phosphorylation through a mechanism that is distinct from the negative signaling pathways associated with NK cell inhibitory receptors for major histocompatibility complex class I molecules (22). These facts prove that HCV-E2–mediated inhibition of NK cells is an efficient HCV evasion strategy, which involves targeting the early antiviral activities of NK cells and allowing the virus to establish itself as a chronic infection.

We have explored whether CD81 cross-linking–induced inhibitory effects occur even in IL-2–stimulated NK cells. CD81 cross-linking by a mAb specific for CD81 inhibited antitumor cytotoxicity and anti-HCV activity mediated by resting NK cells, but this manipulation did not alter both these activities of IL-2–stimulated NK cells (Supplemental Figure 4). This indicated that exposure to IL-2 before CD81 cross-linking abrogates subsequent inhibitory signals in the NK cells. This would be one mechanism whereby the adoptive immunotherapy with IL-2/OKT3–treated liver lymphocytes inhibited HCV replication at the early phase of infection after LT.

Although the role of NK cells in controlling HCV infection and replication has not been completely elucidated, a recent report has indicated that NK cells do not exert a direct cytolytic effect on the HCV replicon–containing hepatic cells but release IFN-γ, suppressing HCV RNA expression (11). The role of IFN-γ in the expression of NK cell–mediated anti-HCV activity has been proved by the observa-